PhD Thesis (extract):
Multi-Scale Modeling and Variability in Cardiac Cellular Electrophysiology

Michael Peter Éamon Clerx

April 24th, 2017

CHAPTER 5

Variability in the dynamical properties of human cardiac I_{Na}

This chapter is based on:

Michael Clerx, Roel L.H.M.G. Spätjens, Cristina Altrocchi, Sandrine R.M. Seyen, Pieter Collins, Enno de Lange, Ralf L.M. Peeters, Paul G.A. Volders (2016). Variability in the dynamical properties of human cardiac I_{Na}. *Manuscript in preparation.*

Michael Clerx, Pieter Collins, Paul G.A. Volders (2015). Applying novel identification protocols to Markov models of I_{Na}. Presented at *Computing in Cardiology, Nice 2015*. Volume 42, pages 889–892.

Abstract

Recent work has shown the increased predictive power of cardiac action-potential models that include variability in their parameters. Yet quantitative data on variability in the kinetics of ionic currents is scarce. We investigated and quantified variability in one of the major ionic currents, the cardiac fast sodium current I_{Na}. Using a simple voltage step experiment, we found that time constants of inactivation varied between roughly one-half and twice the most common value. This suggests that a skewed, perhaps lognormal, distribution is appropriate when modeling variability in time constants. Time constants of fast and slow inactivation were linearly correlated (R=0.66). Next, we performed a literature review and found that midpoints of activation and inactivation were reported over a 40mV range. Midpoints of activation and inactivation were both approximately normally distributed. Midpoint of activation and inactivation showed a linear correlation (R=0.82) and linear regression suggested an average distance of approximately 40mV between midpoints. Fluctuations in the distance between midpoints also appear approximately normally distributed. By reviewing the literature on sources of variability in patch-clamp experiments such as temperature, time since membrane rupture and liquid junction potential, we showed that the observed variability exceeds that which can be expected from experimental conditions alone. Finally, we used computational models to show that the observed variability affects the cellular action potential, and leads to variability in the automaticity of isolated Purkinje cells.

Contents

5.1 Introduction

Variability in the maximum conductance and in the dynamical properties of cardiac ion channels has been linked to critical differences in the response to antiarrhythmic drugs (Sarkar et al., 2012; Britton et al., 2013), and may be a factor explaining the diverse arrhythmias sometimes observed between different carriers of the same mutation (Remme et al., 2008; Weiss et al., 2012, 2015). Incorporating variability into models of the action potential (AP) has been identified as one of the key challenges in the future of cardiac cellular electrophysiology (Abriel et al., 2013) and was the subject of a white-paper featured recently in the Journal of Physiology (Mirams et al., 2016). Yet, studies with an experimental basis that quantify the variability in even the major cardiac ion currents are scarce.

In the present study, we have investigated variability in the kinetical parameters of the cardiac fast sodium current I_{Na}, which is responsible for the initial rapid upstroke of the AP, and plays a major role in AP propagation. Abnormalities in I_{Na} have been linked to long-QT syndrome (type 3), Brugada syndrome, cardiac conduction disease, atrial and ventricular fibrillation, 'overlap syndromes' and more (Amin et al., 2010). While some studies of variability in ionic currents have focused entirely on changes in maximum conductance (Sánchez et al., 2014; Chang et al., 2015; Passini et al., 2016), others have shown the predictive power of including variability in kinetic parameters such as time constants of (in)activation (Romero et al., 2009; Sarkar and Sobie, 2011; Britton et al., 2013). In contrast to changes in maximum conductance, which can be explained by variable ion channel expression levels and measured using protein counting techniques, measuring variability in kinetics requires cellular-electrophysiological experiments and a careful analysis of the experimental factors influencing these results.

Our study proceeds in three parts. First, we perform simple voltage-step experiments and fit a mathematical model to the results to quantify variability in the time constants of inactivation. With these experiments we show that variability between cells occurs even under controlled conditions. Next, we conduct a review of previously reported midpoints of activation and inactivation. This provides an insight into the variability in repeated measurements in and between different laboratories, over a time span of several years. Finally, we incorporate the observed variability into computational models and show the effect of variability on the AP of ventricular and Purkinje cells. By comparing our results to estimates of the uncertainty due to experiment and analysis, we argue that this variability is not experimental noise but an inherent property of the channels. A graphical overview of the study is given in Fig. 5.1.

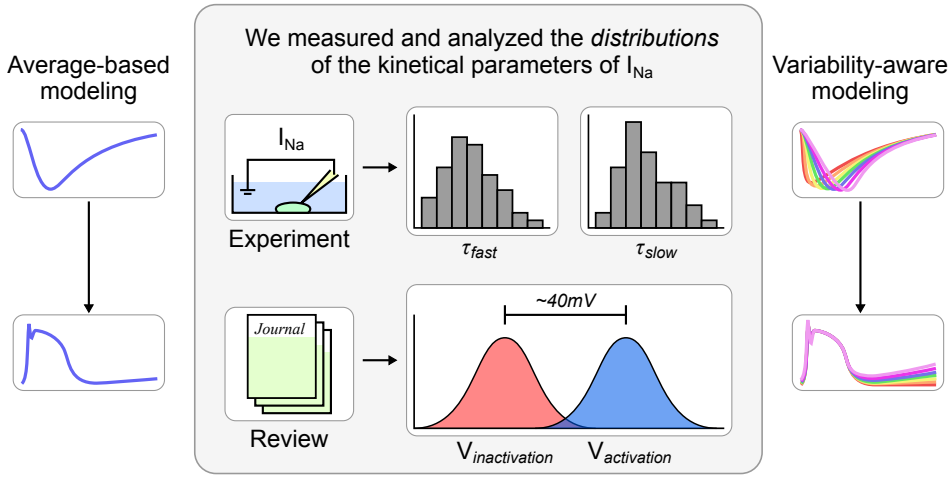

Figure 5.1: Graphical overview of this study. We performed patch-clamp experiments to characterize and quantify variability in the time constants of I_{Na} inactivation, after transfection of wild-type *SCN5A*. Next, variability in midpoints of activation and inactivation was studied by reviewing the existing literature. With this knowledge in hand, we can move from conventional average-based modeling to variability-aware modeling, which predicts not just a single outcome but a biologically realistic range of outcomes.

5.2 Methods

5.2.1 Experimental set-up

To determine whether variability could be observed in a simple, well-controlled experiment, we investigated the currents elicited by applying a single voltage step to cells expressing human *SCN5A*. To quantify the results, a Hodgkin-Huxley style model was fit to the data using whole-trace fitting, which gives more reliable results than the conventional 'disjoint' method of analysis (Willms et al., 1999). Based on the results of an analysis by Walch and Eisenberg (2015), we concentrated on the time constants instead of the steady-states, as the latter cannot be determined uniquely (i.e., variability in fitted parameters may be observed even for identical currents) unless the initial state of the system is known exactly. Finally, we chose to focus on inactivation alone because the membrane-charging process can interfere with recordings of I_{Na} activation (Sherman et al., 1999). A further description of the last two points is provided in the Supplement.

5.2.2 Electrophysiological measurements

Chinese hamster ovary (CHO) cells were cultured in 35 mm dishes with Ham's F-12 medium, supplemented with 10% fetal calf serum and 1% penicillin/streptomycin. Cells were transiently transfected with human WT *SCN5A* (NCBI reference sequence NM_000335.4, isoform b) and green-fluorescent protein (2.5μg pIRES-WT-SCN5A-GFP) using Fugene 6 (Promega

Benelux, Leiden, The Netherlands) as transfection agent. Fluorescence was boosted by adding an additional 0.25μg of DNA coding for fluorescent protein (0.25μg pIRES-empty-GFP).

The cells were then incubated for 24 hours at 37°C, briefly trypsinized and washed twice in culture medium. They were then placed on an inverted microscope in a bath perfused continuously with a solution containing (in mmol/L): 145 NaCl, 4 CsCl, 1 $MgCl_2$, 1.8 $CaCl_2$, 10 HEPES, and 11.1 glucose (pH=7.4 with CsOH). Pipettes were filled with (in mmol/L): 10 NaCl, 120 CsCl, 20 TEACl, 5 MgATP, 5 EGTA, and 5 HEPES (pH=7.2 with CsOH). Patch pipettes were pulled and fire-polished using a DMZ-Universal-Puller (Zeitz-Instruments Vetriebs GmbH, Martinsried, Germany) from 2mm borosilicate glass capillaries (Science Products GmbH, Hofheim, Germany). Experiments were performed at room temperature, which was measured as 22 ± 1.5°C.

Data was collected using three set-ups: An Axopatch 200B amplifier, Digidata 1322A digitizer and Clampex 8.2.0, an Axopatch 200B amplifier, Digidata 1440A digitizer and Clampex 10.2.0, and an Axopatch 1D amplifier, Digidata 1322A digitizer and Clampex 8.2.0 (all Molecular Devices, Sunnyvale, CA, USA). Green fluorescent protein was used to identify cells with successful transfection, which were then patch-clamped in the whole-cell configuration. Access resistance was below 8MΩ for all cells. Cell capacitances ranged from 5.5pF to 47pF. Series resistance compensation (60 to 80%) was employed, with 'prediction' enabled on the amplifiers that provided this (see Sherman-Gold and Maertz, 2012). Data was filtered at 1kHz using the analog low-pass 4-pole Bessel filter on the amplifiers and subsequently digitized at 20kHz.

Directly after rupturing the membrane, cells were stimulated repeatedly with a single voltage step, until the observed peak current had stabilized. Subsequently, a protocol with increasing voltage steps was run (used to characterize voltage-dependent activation). From this data the current elicited by a step from −120mV to −20mV was extracted. All steps were preceded by a few seconds at −120mV to inactivate the channels.

Capacitance artefacts were filtered digitally by omitting data from the first t_a milliseconds after each change in potential. The value for t_a was set manually for each recording, and was in the order of 0.5ms. To estimate the leak in each signal, we fit a simple biexponential curve to the decaying part of the current: $I_{\mathrm{fit}} = I_{\mathrm{leak}} + c_1 e^{-t/\tau_1} + c_2 e^{-t/\tau_2}$. Here, I_{leak}, c_1, c_2, τ_1 and τ_2 were cell-specific parameters that were determined by minimizing the sum-of-squares error between I_{fit} and the recorded I using a downhill simplex method (Nelder and Mead, 1965). The entire signal was then corrected by subtracting the estimated I_{leak}.

5.2.3 Quantifying time constants of inactivation

To quantify differences between experimental recordings, a Hodgkin-Huxley style model of I_{Na} was fit to each recording. We used the equations by Beeler and Reuter (1977), but without the constant term g_{NaC} that was intended to capture background sodium current. The resulting model includes slow and fast inactivation, and has the form:

$$I_{\mathrm{Na}}(t) = m^3 \cdot h \cdot j \cdot g \cdot (V - E) \tag{5.1}$$

$$dm/dt = (m_\infty(V,p) - m)/\tau_i(V,p) \tag{5.2}$$

$$dh/dt = (h_\infty(V,p) - h)/\tau_h(V,p) \tag{5.3}$$

$$dj/dt = (j_\infty(V,p) - j)/\tau_j(V,p) \tag{5.4}$$

Here, g is the fixed maximum conductance, V is the membrane potential and E is the reversal potential for I_{Na}. The model has a single activation variable m, a fast inactivation variable h and a slow inactivation variable j. After a change in membrane potential, each of these variables approaches a voltage-dependent steady state (m_∞, h_∞ and j_∞) with a speed determined by its time constant (τ_m, τ_h and τ_j). The steady states and time constants are all functions of V and a vector of parameters p. When $m_\infty(V,p)$ is plotted against voltage it forms a sigmoid curve and the voltage at which it passes through 0.5 is the midpoint of activation. The midpoint of inactivation is the voltage at which $h_\infty(V,p)$ passes through 0.5. We used the equations for the steady states and time constants from Beeler and Reuter and rewrote them in a parametrizable form, leading to a model with 16 parameters (not including the reversal potential E or maximum conductance g). The complete equations are given in Section 5.A.

When a voltage step is applied to a cell, its membrane potential approaches the applied command potential in a process well approximated by:

$$\frac{dV}{dt} = \frac{V_{\mathrm{cmd}}(t) - V}{\tau_{\mathrm{c}}} \tag{5.5}$$

where $V_{\mathrm{cmd}}(t)$ is the desired command potential, V is the actual membrane potential and τ_{c} is a time constant dependent on the membrane capacitance, series resistance, and amplifier series-resistance compensation settings (Sigworth, 1995). For I_{Na}, this charging time is in the same order as the time constant of activation, even when applying series-resistance compensation (Sherman et al., 1999). We therefore included V_{cmd} in our model as an instantaneous voltage step and modeled V using the above equation. The time constant of the compensated charging process τ_c was added as an additional model parameter to be estimated in our model fitting procedure (see also Clerx et al., 2015).

Model parameters were estimated from measured currents by minimizing a score function $f(p) = \sum_t \left[I_{\mathrm{sim}}(p) - I_{\mathrm{ref}}\right]^2$, where the sum was taken over all sampled instances. Function

minimization was performed using a parallelized particle swarm optimization (PSO) method (Eberhart and Kennedy, 1995). This method requires no derivatives, can deal well with non-smooth functions, and has been reported to perform well on ion-channel model fitting tasks (Loewe et al., 2013, 2016). PSO uses many (pseudo-)random steps, which means it may not always return the same value when re-applied, especially on noisy data. Our parameter vector included the 16 parameters determining the model's time constants and steady states, the maximum conductance g, and the membrane charging time constant τ_c. The reversal potential E was held constant at $E = 50\mathrm{mV}$. A small number of heuristic modifications were made to the score function to ensure good fits for all cells: First, based on our analysis of the error introduced by the slowly charging membrane, we fit only to the signal starting approximately halfway into the initial downslope. Next, we added a number of constraints to ensure the variables took on the role of activation and (fast and slow) inactivation. We used $m_\infty(-20, p) \geq 0.5$, $h_\infty(-20, p) \leq 0.5$ and $j_\infty(-20, p) \leq 0.5$ and constrained the time constants with $\tau_m(-20, p) < \tau_h(-20, p) < \tau_j(-20, p)$ and the heuristics $\tau_h/\tau_m \leq 75$ and $\tau_j/\tau_m \leq 400$.

5.2.4 Computational methods

Simulations of the cellular AP were performed using the human ventricular model by Grandi et al. (2010) and the human Purkinje model by Stewart et al. (2009). Both models include an I_{Na} formulation based on the human ventricular model by ten Tusscher and Panfilov (2006). All simulations were carried out using Myokit (see Chapter **??**). Patch-clamp data preprocessing and ion-current model fitting were performed using Myokit and NumPy/SciPy (Jones et al., 2001).

5.2.5 Review of midpoints of (in)activation

In the second part of our research, we conducted a review of published midpoints of activation and inactivation of I_{Na}. These midpoints are widely reported, allowing a large number of experiments to be compared. In addition, they are measured and calculated in a more uniform way than time constants or other channel characteristics. Peak current was not investigated as it varies strongly with channel density, activation and inactivation kinetics, and measurement factors such as temperature, sampling rate, and the applied voltage protocol.

Published recordings of I_{Na} in human myocytes are limited, with notable exceptions being Sakakibara et al. (1992); Schneider et al. (1994); Feng et al. (1996) for atrial myocytes and Sakakibara et al. (1993) for ventricular cells. By contrast, studies with cloned human sodium channels in expression systems are far more common. Typically, these studies investigate the changes caused by a mutation, but also report midpoints measured with wild-type (WT) DNA. This allowed us to collect a large number of reports of WT midpoint of activation

Table 5.1: Collected reports of either midpoint of activation, midpoint of inactivation or both, split by α-subunit. Where possible, GenBank accession numbers are provided. The total number of reports using each α-subunit is given as N. For every subtype, the number of reports made with β1-subunit co-expression is given as β1. Finally, the number of reports N (with and without β1-subunit) is broken down according to the expression system used (HEK293 or tsA201, Xenopus oocytes and CHO cells). The totals for each subgroup are given on the bottom row.

Code	**Description**	**Acc. No.**	**N**	**β1**	**HEK**	**Ooc.**	**CHO**
a	Isoform a (Q1077)	AC137587	25	4	23	0	2
b	Isoform b (Q1077del)	AY148488	28	7	23	1	4
a*	hH1 (R1027Q)	M77235	67	42	49	16	2
b*	hH1a (T559A; Q1077del)	None	6	3	6	0	0
?	Unknown	None	41	24	38	2	1
			167	80	139	19	9

and inactivation.

Table 5.1 shows the number of reports from expression system experiments collected in our study. The pore-forming, α-subunit expressed in these experiments differed slightly, and included the 2016 amino-acid long reference sequence (isoform a), the naturally more common isoform with a deletion at position 1077 (isoform b) and variants of both a and b with a slight variation not commonly found in human DNA, which we dubbed a* and b* (Makielski et al., 2003; Ye et al., 2003). In addition, we included experiments with and without the β1-subunit, made in human embryonic kidney (HEK) cells (including tsA201), Xenopus oocytes or CHO cells. The complete list of publications is given in Section 5.C.

All reported midpoints included in our analysis were specified as (1) the mean midpoint of (in)activation, (2) the corresponding number of measurements (i.e., the number of cells) and (3), the corresponding standard error of the mean (SEM). Using this data, we calculated the standard deviation (SD) for each report and constructed a probability density function (PDF) assuming that the measurements in each report followed a normal distribution. The different PDFs were then multiplied by the number of measurements, discretized (so that they resembled fine-grained histograms) and summed to create the combined PDFs seen in Fig. 5.5.

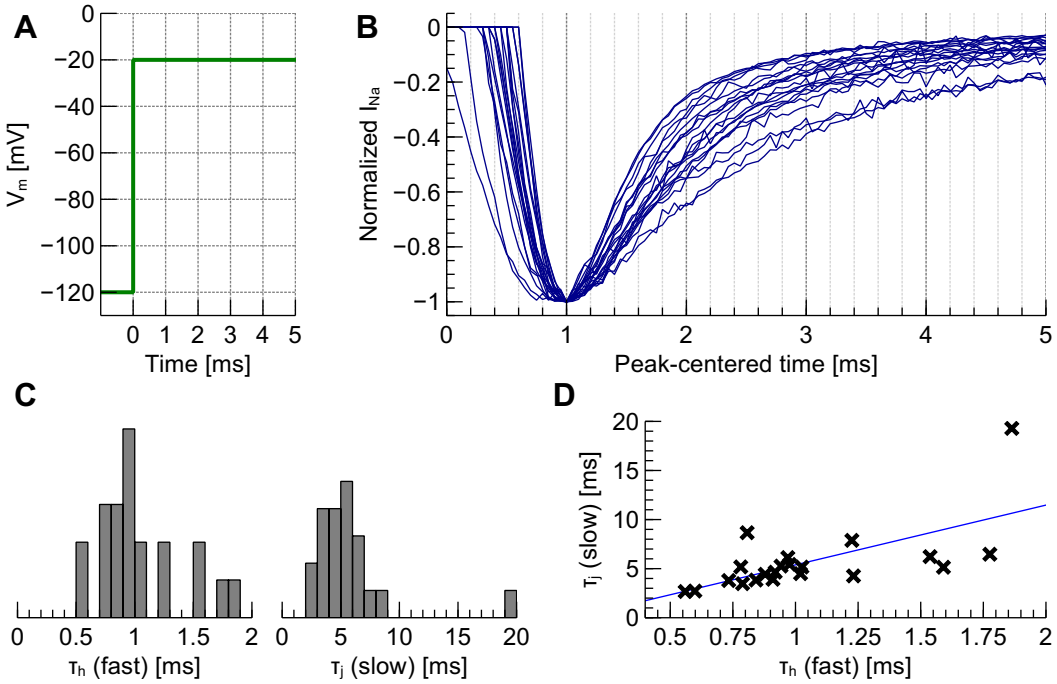

Figure 5.2: (*A*) A simple step protocol from −120mV to −20mV. (*B*) The resulting I_{Na}current, measured in 21 cells. All data was leak-corrected and had the capacitance artefacts removed, leading to the initial flat (zero) response. Data was time-shifted so that the peak occurred at $t = 1$ms. (*C*) Time constants of fast and slow inactivation, measured by fitting models to the data from each cell. (*D*) The correlation between the time constants of fast and slow inactivation.

5.3 Results

5.3.1 The time constants of inactivation vary from cell to cell

Fig. 5.2.B shows the current measured in 21 cells, normalized to a peak current of −1, and time-shifted to have its peak at $t = 1$ms. The initial downward slope and the time to peak varies from cell to cell (see also the alternative views in Section 5.B.1). Once the peak is reached, the current inactivates with a time course that varies from cell to cell. This variability was quantified by fitting a model of I_{Na}, and the resulting time constants of fast and slow inactivation are shown in Fig. 5.2.C. The distribution appears skewed, possibly lognormal, with values ranging from about half to twice the most common value (or mode), although the distribution for slow inactivation shows an outlier at around 4 times the mode.

5.3.1.1 Slow and fast inactivation are not independent

Fig. 5.2.D shows the relation between the slow and fast time constants. A moderate linear correlation was found, with a Pearson correlation coefficient $R = 0.64$. Linear regression

yielded $\tau_j \approx -0.7 + 6.1\tau_h$. The small offset suggests that perhaps the relation between the time constants is best expressed as the ratio τ_j/τ_h. Calculated per cell, this had a mean of 5.4 and a standard deviation of 1.9.

5.3.1.2 The time constants do not correlate with time since rupture

The time between membrane rupture and application of the step protocol varied between the experiments. It is possible that slow changes in membrane potential occurred during this time, e.g., due to a drifting liquid junction potential (Hanck and Sheets, 1992). Fig. 5.3 shows that the largest and smallest time constants were all measured around 500ms after membrane rupture, and there is no clear correlation between time since rupture and the time constants (Pearson correlation coefficient -0.039 for τ_h and time, 0.082 for τ_j and time). In addition, we obtained recordings at a second point of time for a subset of cells but generally saw only small differences between both measurements (see Section 5.B.1).

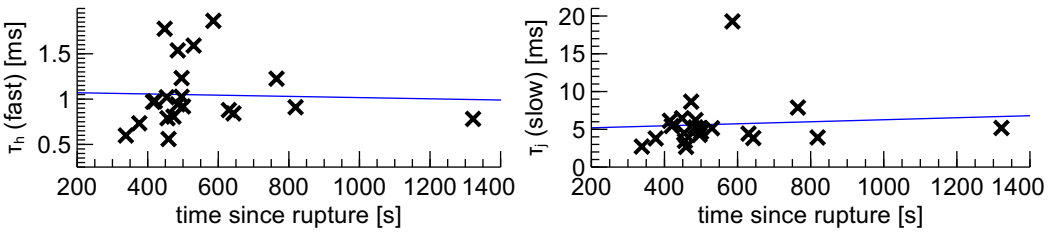

Figure 5.3: The fast (τ_h) and slow (τ_j) time constants of inactivation, plotted against the time between rupturing the membrane and performing the voltage step and current measurement. No clear relation between the time and the time constants can be seen, as indicated by the almost horizontal regression lines.

5.3.1.3 The influence of noise is limited

We estimated time constants by searching for the values that gave the best fit to our data using a pseudo-randomized approach (see Section 5.2.3). However, in the presence of noise, this procedure may not return a unique result, as multiple parameter sets can be found that will give different but almost equally good results, so that the 'best fit' chosen depends on details of the algorithm and score function used, rather than the underlying biology. To investigate the resulting noise-induced variability, we ran the analysis procedure several times for each cell. Because our dataset contained 21 cells, we performed 21 fits per cell so that the variability between cells and between fits could more easily be compared.

Fig. 5.4 shows the values obtained this way for each cell, alongside the values obtained by a single fit to each cell. For most cells, the variability between repeated fits was far smaller than the variability between cells. A numerical analysis supports this observation. Between cells, τ_h had a mean of 1.0ms and a standard deviation of 0.36ms, while the mean and standard deviation for τ_j were 5.7ms and 3.4ms respectively. The mean standard deviation

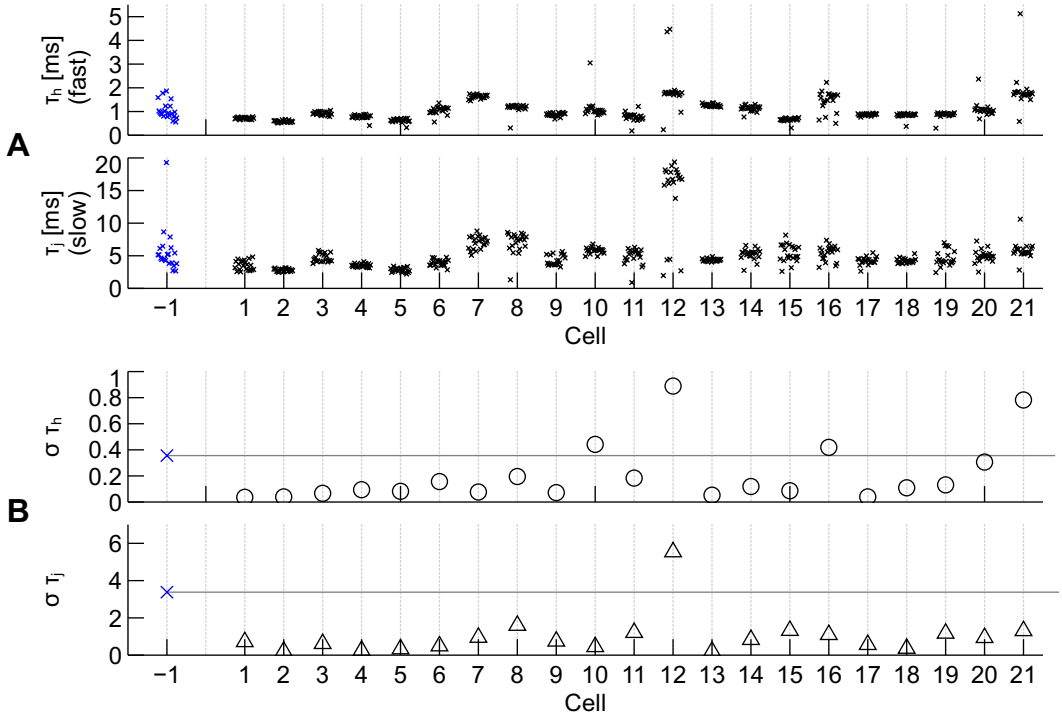

Figure 5.4: **Variability between cells exceeds variability in repeated fits.** (*A*) Fast (*top*) and slow (*bottom*) time constants of inactivation. The data points at position -1 each represent a single fit to a different cell. The subsequent signs at position 1, 2, 3, etc. indicate the outcomes of repeated fits to cells 1, 2, 3, etc. (*B*) The standard deviation of fits to different cells (position -1) and of repeated fits to the same data (positions 1, 2, 3, etc.).

observed in repeated fits was 0.21ms for τ_h and 0.99ms for τ_j. If we assume both standard deviations (between cells and between fits) describe independent distributions, we can use $\sigma^2_{x+y} = \sigma^2_x + \sigma^2_y$ to correct the inter-cell standard deviations for the fitting error to find $\sigma_h = 0.29$ms and $\sigma_j = 3.2$ms.

5.3.1.4 Variability is not explained by temperature

Temperature was kept within a ±1.5°C bracket during the recordings. If temperature alone induced the observed variability, this should cause the ratio between our highest and lowest time constants to be $0.5^{-3/10} \approx 1.23$, for both slow and fast inactivation (Nagatomo et al., 1998). However, the ratio seen in our data was closer to 4 for both, suggesting temperature differences may partly, but not fully explain the observed variance.

5.3.2 The midpoints of (in)activation vary from cell to cell

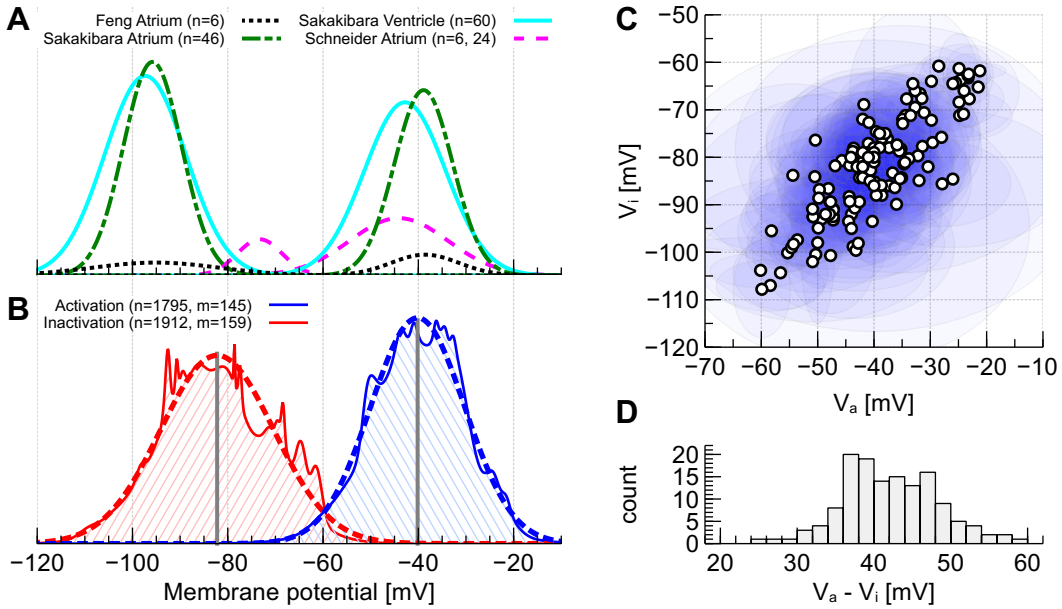

Figure 5.5: (*A*) The midpoints of activation and inactivation reported in human myocyte studies on n cells. All four studies show large variability, represented here as a normal curve with the reported mean and standard deviation, and an area under the curve equal to the number of measured cells. (*B*) Distribution of reported midpoints of activation and inactivation based on measurements in expression systems. The shaded areas shows the summed distribution constructed from the reported data for n cells in m individual reports. The thick dashed lines indicate a normal distribution with the corresponding mean and SD. The vertical grey lines indicate the mean of the inactivation and activation distributions. (*C*) Correlation between reported midpoints of activation (V_a) and inactivation (V_i), shown for studies that reported both. The white dots indicate a reported pair of mean midpoints, with the corresponding $\pm 2\sigma$ range indicated by the blue ellipses. (*D*) A histogram of the difference between midpoints of activation and inactivation.

Fig. 5.5.A shows the distributions of V_i and V_a obtained from studies with human myocytes, one with ventricular myocytes and three with atrial samples. All studies show large variability in outcome, independent of the number of cells being used. Similar variation was seen in the expression system data. In these reports, the standard deviation of V_a ranged from 0.4mV to 22mV, with a mean standard deviation of 4.5mV. Standard deviations of V_i ranged from 0.13mV to 15mV, with a mean of 4.0mV. Assuming a normal distribution, this indicates a spread of ±8mV (95% interval) is not uncommon in a single run of experiments.

5.3.2.1 The mean midpoints of (in)activation vary from study to study

Fig. 5.5.B shows the distribution of cellular V_a and V_i constructed by summing the distributions from multiple studies. Both distributions show a spread of approximately ±20mV (95% interval), indicating a much larger variance between studies than within studies. Even the smaller peaks, which indicate the means of individual reports, occur over a range of ±20mV

for both activation and inactivation. Both reconstructed distributions are reasonably well approximated by a normal distribution.

5.3.2.2 The midpoint of activation and inactivation are not independent

Fig. 5.5.B shows the distributions for V_i and V_a overlap. However, physiologically it seems likely some distance between V_i and V_a is required and that the two distributions are not independent. Fig. 5.5.C shows the midpoint of inactivation plotted against the midpoint of activation from the same study. Studies reporting only the midpoint of activation or only inactivation had to be omitted for this figure, but no other filtering was performed, leading to a total of 138 data points. A strong linear correlation is seen between the reported midpoints of activation and inactivation (Pearson correlation coefficient R=0.82). Using unweighted least-squares based linear regression, we found an offset of −42.06mV and a slope of 1mV/mV (1.000046).

To separate the simultaneous variance of V_a and V_i from their individual variance, we calculated the quantity $V_a - V_i$ (using only the means, not the reconstructed distributions) and plotted its distribution in Fig. 5.5.D. Here, we found a standard deviation of 6.3mV (the corresponding standard deviations for V_a and V_i in this dataset were 8.8mV and 10.8mV respectively). This indicates that, despite their strong linear relation, both midpoints also fluctuate independently.

5.3.2.3 Cell-type and channel-variant do not explain study-to-study variability

Fig. 5.5.B incorporates data from all reports included in our analysis, and so contains data from different expression systems, with and without the β1-subunit and with slightly different α-subunits. To remove these influences, Fig. 5.6.A was made using only data from the largest subgroup: The a* α-subunit, co-expressed with β1-subunit in HEK cells. As can be seen, this created a slight shift in the mean of the distribution, but did not significantly reduce the observed spread. A quantitative view of the midpoint data is given in Table 5.2. This table shows the mean V_a and V_i for the combined data, as well as for various subgroups. Here it can be seen that, while the standard deviation of V_a is slightly smaller in the biggest subgroup, the standard deviation of V_i is actually increased.

α-subunit: Fig. 5.6.B shows the data split by α-subunit. Papers that did not explicitly mention the subunit used were excluded for this figure. Note that the number of reports (m) and the number of cells (n) varies between the subgroups. The number of reports for isoform b* in particular may be too low for a good estimate of the real distribution. Interestingly, the means of the distributions do not differ strongly between subgroups. The groups with the largest number of measurements show the largest spread, indicating that either these cohorts are still too small to estimate the underlying distribution or that larger groups are more prone to capture the effects of some underlying confounding factors.

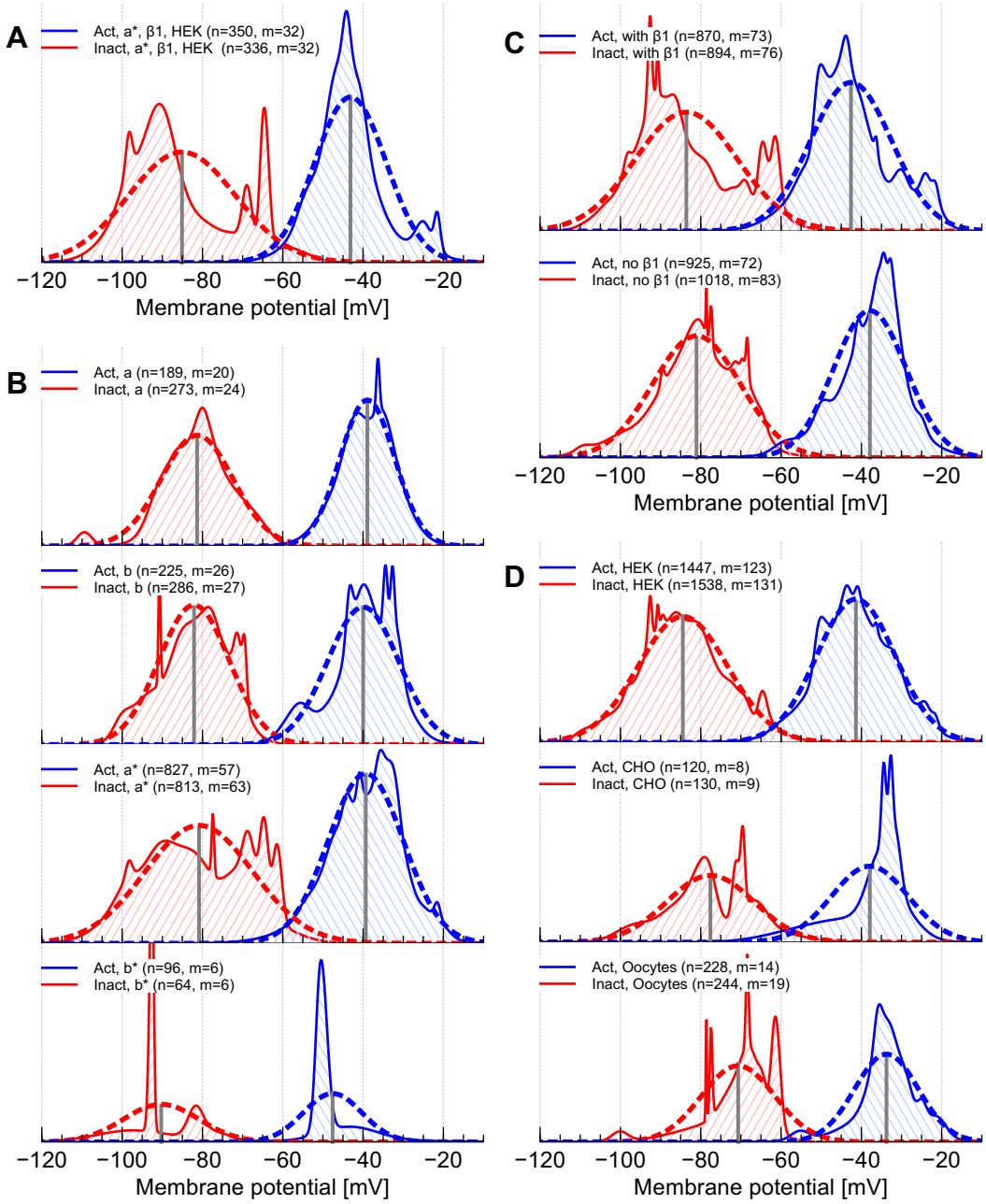

Figure 5.6: (*A*) Reconstructed distribution of midpoints of activation (red) and inactivation (blue) for the largest subgroup (a* α-subunit, with β1-subunit, expressed in HEK cells). The shaded areas indicate the summed distributions. The dashed lines indicate normal distributions with the equivalent mean and standard deviation. The mean is indicated by the solid grey line. (*B*) The distributions split by α-subunit: a (Q1077), b (Q1077del), a* (R1027Q) and b* (T559A; Q1077del). (*C*) The distributions split by co-expression of β1-subunit. (*D*) The distributions split by expression system.

Table 5.2: Ranges of midpoint of activation (left) and inactivation (right). The subgroup mean midpoints of activation and inactivation are indicated as μ_a and μ_i respectively, with the corresponding standard deviations shown as σ_a and σ_i. The 2-sigma range around each mean is shown in the columns $r_{2\sigma,a}$ (activation) and $r_{2\sigma,i}$ (inactivation). For each subgroup, the number of reports (m) and total number of measurements (n) is given.

	Activation					Inactivation				
	μ_a	σ_a	$r_{2\sigma,a}$	m	n	μ_i	σ_i	$r_{2\sigma,i}$	m	n
Combined	-40.2	9.88	-59.9, -20.4	145	1795	-82.2	11.8	-106, -58.5	159	1912
HEK, a*, β1	-43.1	8.90	-60.9, -25.3	32	350	-85.1	13.3	-112, -58.4	32	336
Isoform a	-38.9	6.79	-52.5, -25.4	20	189	-81.3	8.95	-99.2, -63.4	24	273
Isoform b	-40.0	8.86	-57.7, -22.3	26	225	-82.1	8.74	-99.6, -64.6	27	286
Isoform a*	-39.3	9.3	-58.0, -20.6	57	827	-80.8	13.4	-108, -53.9	63	813
Isoform b*	-47.6	7.28	-62.1, -33.0	6	96	-90.3	9.38	-109, -71.5	6	64
Unknown	-40.7	11.9	-64.5, -16.8	36	458	-84.1	11.6	-107, -60.9	39	476
With β1	-42.6	10.1	-62.9, -22.3	73	870	-83.6	12.7	-109, -58.2	76	894
Without β1	-37.9	9.04	-56.0, -19.8	72	925	-81.0	10.9	-103, -59.2	83	1018
HEK	-41.4	9.76	-60.9, -21.8	123	1447	-84.5	11.1	-107, -62.2	131	1538
CHO	-37.9	9.54	-57.0, -18.8	8	120	-77.6	10.9	-99.3, -55.9	9	130
Oocyte	-33.7	7.90	-49.5, -17.9	14	228	-70.1	9.10	-88.9, -52.5	19	244

Inclusion of β1-subunit: Fig. 5.6.C shows the distributions of midpoints with and without the β1-subunit. Papers that did not explicitly mention co-expression of the β1-subunit were assumed to fall into the 'no β1-subunit' category. Here, the means seem to indicate a shift to more negative potentials when the β1-subunit is co-expressed (-4.7mV for activation, -2.6mV for inactivation, see Table 5.2). However, the minimum and maximum values reported do not reinforce this pattern.

Expression system: Fig. 5.6.D shows the influence of the expression system on the measured midpoints. The overwhelming majority of measurements were performed using HEK cells, making the resulting distributions difficult to compare. However, it seems measurements in HEK cells and CHO cells are comparable, whereas oocyte experiments show a shift towards the positive.

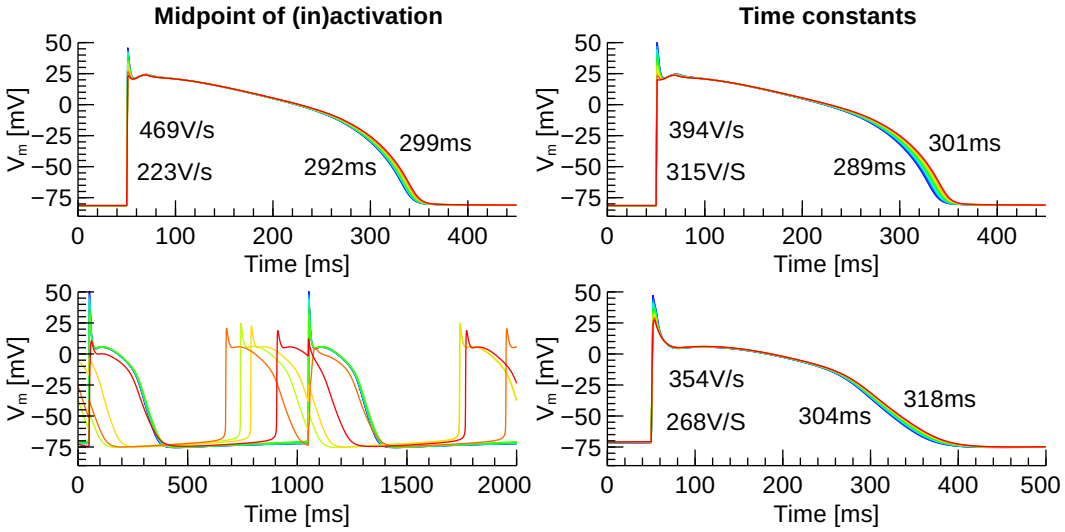

Figure 5.7: Simulations of the ventricular (*top*) and Purkinje (*bottom*) AP, incorporating variability in the midpoints of activation and inactivation (*left*) and time constants of inactivation (*right*). In all cases, the size of the initial upstroke and action potential duration were affected. In the Purkinje model, varying the midpoint of inactivation and activation also affected the cells' automaticity.

5.3.3 The observed variability affects the cellular AP

To investigate the effects of the observed variability on the cellular AP, we ran simulations using a model of the human ventricular AP and the Purkinje AP. In a first simulation, we varied the midpoints of activation and inactivation simultaneously (reflecting their strong linear correlation) by −5mV to +5mV in 1mV steps. The results are shown in the left panels of Fig. 5.7. In both models, this had a strong effect on the maximum upstroke velocity (even doubling it in the ventricular model) and a smaller effect on the action potential duration (APD). In the Purkinje cell model, moving the midpoints of (in)activation also lowered the threshold for activation, leading to automaticity at higher frequencies, causing the cells to depolarize ahead of the pacing signal.

In a second simulation, we varied both time constants of inactivation simultaneously from 0.5 to 2 times the original value in 11 logarithmically spaced steps. This had a much smaller effect on the upstroke velocity in both models, but a greater effect on the APD. Purkinje automaticity was unaffected by changes to the time constants. In all simulations, models were pre-paced at 1s intervals for 1000 beats after each change to the parameters.

5.4 Discussion

Despite the importance of including cell-to-cell variability in the parameters of computational models of the cardiomyocyte AP, data on such variability is scarce. In this study, we showed new evidence of variability in the time constants of inactivation in I_{Na} and reviewed existing evidence for variability in the midpoints of (in)activation. Using models of ventricular and Purkinje AP, we showed that variability has an impact on the shape and duration of the cellular AP.

5.4.1 Time constants of inactivation

We observed a variability between time constants of inactivation that is larger than can be expected from experimental sources of error alone. Hanck and Sheets (1992) showed the time between rupture of the cell membrane and performing the experiment could affect the time constants measured in Purkinje cells. However, we saw no correlation of our measurements with the time between rupture and experiment in our CHO cell measurements. Similarly, Abriel et al. (2001) saw no correlation in HEK cell recordings. Noise in the recordings was quantified using a repeated-fit strategy, and found to explain only a small part of the observed variability. Temperature is known to affect measurements of time constants of I_{Na}, but we saw a larger variance than would be predicted based on the results of Nagatomo et al. (1998), while the data of Keller et al. (2005) would suggest an even smaller temperature-based variation. Other factors, such as the internal and external solutions used, were constant throughout our experiments. We note also that, near -20mV, the time constants of inactivation are weakly voltage-dependent (see for example Beeler and Reuter, 1977), so that any factor leading to small transient changes in the potential across the channel will not have a strong influence. Taken together, these findings suggest the origin of the observed variability was not experimental error, but a fundamental feature of I_{Na} in expression systems.

Table 5.3 shows that the standard deviations in our measurements closely match those of previous studies in expression systems and isolated cardiomyocytes. The means too, are very similar to those reported by Wan et al. (2001) in HEK cells, but both fast and slow time constants are approximately half the value found in myocytes by Sakakibara et al. (1992, 1993). While we cannot see the shape of the distribution of the time constants in these publications, the size of the standard deviations suggests that our results are representative for this type of experiment.

5.4.2 Midpoints of activation and inactivation

Some measure of cell-to-cell variability was seen in all reviewed reports of the midpoints of (in)activation, with a mean standard deviation of approximately 4mV and a maximum of

Table 5.3: Time constants of inactivation at −20mV.

	$\mu_{fast}(\tau_h)$	σ_{fast}	$\mu_{slow}(\tau_j)$	σ_{slow}	
This study	1.0	0.36	5.7	3.4	CHO cells
Wan et al. (2001)	0.79	0.34	5.1	1.6	HEK cells
Sakakibara et al. (1992)	2.6	0.40	12	2.8	Atrial myocytes
Sakakibara et al. (1993)	2.1	0.47	12	3.3	Ventricular myocytes

15mV for V_i and 22mV for V_a. Assuming a normal distribution, this would lead to a range of 16mV within two standard deviations of the mean, within the average study. Note that systematic errors made within a single laboratory would not show up in this figure, nor would factors such as α-subunit, β1-subunit co-expression, or differences in the internal solution used. Again, temperature fluctuations could play a role. Nagatomo et al. (1998) recorded a shift in the midpoint of activation of +0.43mV per degree Celsius, and a +0.47mV shift for inactivation, but no such shifts were observed by Keller et al. (2005). Even assuming a 0.5mV/°C shift and a bath temperature ranging over 10°C, this would only explain a 5mV difference in midpoints. Time since rupture may also have varied from cell to cell and affected the recordings. In the Purkinje-cell recordings by Hanck and Sheets (1992), the midpoints of (in)activation changed over time with a rate of approximately 0.5mV/min. If a similar phenomenon occurs in expression systems, this could explain a part of the observed variability, if the standard deviation in time-to-experiment was approximately 8min in the average study (i.e., 32min within the 95% interval). However, Abriel et al. (2001) saw no time-dependent shifts in their data measured in HEK cell experiments, which were the predominant form of experiment in our data. In addition, our own data, though perhaps not representative, showed a standard deviation of 3.5min in the time-to-experiment. This suggests there is some measure of inherent variability in the midpoints of (in)activation.

The difference *between* studies extends over a much larger range, with reported mean midpoints varying over a range of 40mV for both activation and inactivation (see Fig. 5.5.C). In contrast to variability *within* studies, this variability may be partially explained by systematic differences between studies and laboratories. However, it is interesting to note that factors such as α-subunit and β1-subunit expression only cause small differences in the mean. Note also that some studies, for example the one by Tan et al. (2005) already report *multiple* mean midpoints, to allow pairwise comparison with mutated currents made under similar seasonal conditions. However, the difference seen between the midpoints in the study by Tan et al. was at most 3mV for activation, and 7mV for inactivation. Further work is needed to clarify the origins of these large inter-study differences.

5.4.3 Correlation between kinetical parameters

Fig. 5.5.C shows a striking linear correlation between V_i and V_a. A moderate correlation between the fast and slow time constants of inactivation was also found. Such correlations could be caused by some hidden variable affecting both parameters simultaneously. This

could be an experimental error, but is also consistent with the idea of regulation of channel function. However, it is unclear how this would arise, especially in expression systems that do not natively express I_{Na}.

5.4.4 Implications for cardiac modeling

Our results show that variability in the kinetical parameters of I_{Na} exists and has an effect on the AP. For computational studies that include variability in AP model parameters, perhaps the most important finding is that parameters are *correlated*. This implies that variability in the different parameters cannot be simulated by sampling from independent distributions, but that the covariance of the different model parameters must be taken into account. Alternatively, relations such as $\tau_j/\tau_h \approx 5$ and $V_a - V_i \approx 40\mathrm{mV}$ can be exploited to reformulate the parameters in terms of independent random variables. For example, assuming normally distributed midpoints of activation, $V_a = X_1, V_i = V_a + 40 + X_2$, where X_1 and X_2 are variables drawn from a normal distribution. Similarly, assuming lognormally distributed time constants, $\tau_h = Y_1, \tau_j = 5 \cdot \tau_h \cdot Y_2$ where Y_1 and Y_2 are drawn from a lognormal distribution. A further simplification was made in Section 5.3.3, where we set $X_2 = 0$ and $Y_2 = 0$. A physiological meaning can be attributed to these variables: in our example X_1 represents variability in the current's steady-state voltage dependence, while X_2 represents variability in the 'window' that gives rise to the 'window' current.

5.4.5 Implications for reporting of cell-electrophysiological data

The recognition of cell-to-cell variability in channel kinetics has a direct impact on any study investigating I_{Na} channelopathies, and may be a factor explaining phenomena such as ectopic beats in some, but not all, areas of the Purkinje system (for example via increased automaticity such as seen in Section 5.3.3). This has important implications for the way cell-electrophysiological results are reported. For instance, instead of only giving means and standard errors of the mean, data points corresponding to each individual cell should be given (see also Drummond and Vowler, 2011). Ideally, the data points should be labeled per cell so that correlations between the different parameters can be established. Most importantly, based on this study, it appears the variability in kinetical parameters is more than just noise, and could be a relevant physiological parameter.

5.4.6 Limitations

Future work could focus on increasing the sample size of the experiments, which would improve the accuracy of the results. Such a dataset might be obtainable with automated patch-clamp experiments, and could be performed cheaply if run as a baseline test done before a secondary experiment. While we chose to focus on I_{Na}, one of the major cardiac ionic currents, similar investigations into all other currents are needed to gain a full picture

of variability in the processees underlying the cardiac cellular AP.

We simulated the effects of I_{Na} variability on single cells. In tissue, the kinetics of I_{Na} are also likely to affect the conduction velocity and the safety factor of propagation. However, this will depend strongly on whether the coupled cells differ from each other, or if perhaps their shared environment and electrotonic coupling will cause them to function in a similar way.

The presented literature review was based entirely on reported means and standard deviations (calculated from reported standard errors of the mean). Future work could focus on obtaining data from individual cells, which will allow cell-to-cell variability to be reviewed more directly. Since the dataset contains many publications by the same groups, we also cannot exclude the possibility that some cells appear in the dataset more than once, so that the real number of cells is smaller than reported and some points in the distribution are over-represented. It is also possible there are still other confounding factors causing the observed variability in the measured results, that do not occur naturally on the same scale. For example, while the CHO cells we tested were all treated the same way, it is possible that naturally arising differences in stretch affected the ion channel characteristics (Morris and Juranka, 2007). Finally, the exact α-subunit used in a study is not always easy to determine, as many papers do not list an accession number or were written before the existence of variation between available plasmids was widely known.

5.4.7 Comparison to previous work

A study by Pathmanathan et al. (2015) fit multiple models of I_{Na} to data on the steady-state of inactivation in canine datasets, and investigated the effects of the different inactivation curves on the single-cell level. This work focused on the mathematical methodology of incorporating variability in I_{Na}, which contrasts with our focus on identifiability and possible experimental origins of variance. Interestingly, Pathmanathan et al. used two datasets from the same lab but made at different times, and found differences between the two datasets. This matches well with the large inter-study differences seen in our pooled midpoint data, and underscores the need to perform large studies of variability over longer periods of time.

Table 5.2 shows the mean midpoints of activation and inactivation measured in CHO cells occurred at higher potentials than in HEK cells (but note the different sizes of the datasets). This is consistent with earlier findings by Watanabe et al. (2011a) for I_{Na} and Fernandez et al. (2003) for Kv3.3. The collected data on midpoints also allows us to investigate the influence of factors such as the expression system used and co-expression of the β1-subunit. As there is no consistency in the size or direction of the shifts reported by individual studies investigating β1-subunit (see the table in Section 5.B.3) this may provide a useful 'consensus' view of its effects.

5.5 Conclusion

The fast and slow time constants of I_{Na} inactivation show variability that can not be explained by experimental error alone. A review of data reported in the literature suggests this is also the case for the midpoints of (in)activation. Simulations of Purkinje and ventricular electrophysiology show the observed variability has a notable effect on the cellular AP, and may lead to increased automaticity in isolated Purkinje cells. A moderate corelation was seen between the fast and slow time constants of inactivation, and a strong correlation between midpoint of activation and inactivation was observed. This suggests simulations incorporating variability in kinetical parameters should not vary these parameters independently but adapt their modeling strategy to incorporate these correlations. Finally, the recognition of cell-to-cell variability as a biological feature implies it should receive increased attention as a possible arrhythmogenic influence. Consequently, electrophysiological data should be reported in a manner that highlights where cell-to-cell variability and correlations between parameters occur.

Acknowledgments

The work of PGAV is supported by The Netherlands CardioVascular Research Initiative, CVON PREDICT. The authors would like to thank Ronald Wilders, Antoni van Ginneken and Jordi Heijman for our valuable discussions.

5.A Extended methods

The complete equations used to model I_{Na} are given below.

$$I_{\mathrm{Na}}(t) = m^3 \cdot h \cdot j \cdot g \cdot (V - E) \tag{5.6}$$
$$dm/dt = (m_\infty - m)/\tau_i \tag{5.7}$$
$$dh/dt = (h_\infty - h)/\tau_h \tag{5.8}$$
$$dj/dt = (j_\infty - j)/\tau_j \tag{5.9}$$
$$dV/dt = (V_{\mathrm{cmd}} - V)/\tau_{\mathrm{c}} \tag{5.10}$$

Time constants and steady-states (for $x \in \{m, h, j\}$):

$$\tau_x = 1/(\alpha_x + \beta_x) \tag{5.11}$$
$$x_\infty = \alpha_x/(\alpha_x + \beta_x) \tag{5.12}$$

and

$$\alpha_m = (V + p_1)/(1 - \exp(-p_2 * (V + p_1))) \tag{5.13}$$
$$\beta_m = \exp(-p_4 * (V + p_3)) \tag{5.14}$$
$$\alpha_h = \exp(-p_6 * (V + p_5)) \tag{5.15}$$
$$\beta_h = p_9/(1 + \exp(-p_8 * (V + p_7))) \tag{5.16}$$
$$\alpha_j = \exp(-p_{11} * (V + p_{10}))/(1 + \exp(-p_{13} * (V + p_{12}))) \tag{5.17}$$
$$\beta_j = p_{16}/(1 + \exp(-p_{15} * (V + p_{14}))) \tag{5.18}$$

The parameters to be identified were $p_1, p_2, ..., p_{16}, g, \tau_c$. We used $E = 50\mathrm{mV}$, as determined by the internal and external solutions.

Note that for a fixed membrane potential, all time constants and steady-states are constants, so that $p_1, p_2, ..., p_{16}$ can be dropped in favor of $\tau_m, \tau_h, \tau_j, m_\infty, h_\infty, j_\infty$.

5.A.1 Time constants are identifiable

If a model can be made to fit the same data in different ways (i.e., if it gives the same result with different parameter values) it is said to be *unidentifiable*. In such a case, variability in the parameters obtained by fitting a model can not be used to show variability in the underlying process. Walch and Eisenberg (2015) performed a detailed analysis of the identifiability of Hodgkin-Huxley style models, such as the one given above and used in this study. For voltage-step protocols (with constant voltage steps) and long noise-free current recordings, they found that time constants can be uniquely identified but steady-state values are fundamentally unidentifiable.

5.A.2 Membrane charging interferes with activation

When a voltage change is applied to a cell, the membrane potential does not change instantly but requires a short charging time, with a duration dependent on the membrane capacitance and access resistance. For I_{Na}, which can activate and inactivate in well under 5 milliseconds, this is an important effect. Most patch-clamp amplifiers contain compensation circuitry that temporarily injects extra current in an attempt to shorten the membrane charging time (Sigworth, 1995; Sherman et al., 1999). However, since the membrane capacitance varies between cells and the exact amount of compensation used is set using analog controls, this may introduce variability in the recordings.

If no compensation is used, membrane charging can be modeled as a simple capacitor charging circuit. This means that an updated model including membrane charging should be able to recreate currents recorded without compensation exactly. Unfortunately, not using compensation would lead to longer capacitance artefacts resulting in an unacceptable loss of signal. We therefore measured the compensated and uncompensated behavior of our amplifier (Axopatch 200B) to check if compensated behavior could still be approximated well by a simple charging capacitor circuit. To this end, we constructed the model cell shown in Fig. 5.8. It consists of two 22MΩ resistors which represent the access (pipette) resistance encountered in a normal experiment and a single 500MΩ resistor that represents the membrane resistance. A 22pF capacitor is included as a substitute for membrane capacitance. These values are consistent with those given in Sigworth (1995). To measure the model cell's charging time, a patch-clamp amplifier in voltage-clamp mode was attached to terminal A1 and used to perform a voltage step. A second patch-clamp amplifier in a voltage-measuring mode was then attached at terminal A2 and used to measure the potential over the resistor representing the membrane.

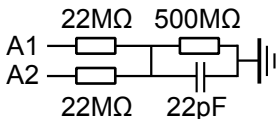

Figure 5.8: The model cell used to investigate the delayed changing of the membrane potential following a voltage step, with and without amplifier compensation.

Fig. 5.9 shows the potential over the model cell during a step from 0mV to 10mV. The recordings reveal a few milliseconds delay at the start of each step, followed by a quick jump in voltage, and finally settling into a simple exponential form. The potential then converges to something very near the desired potential, but not exactly, due to the voltage drop across the series or access resistance. With series resistance compensation enabled, this voltage drop is minimized and the charging process is accelerated. In the traces on the right panel of Fig. 5.9 the voltage drop has been artificially removed by rescaling the potentials. In this

case, we found the process could be well approximated as

$$\frac{dV}{dt} = \frac{V_{\mathrm{cmd}}(t - t_0) - V}{\tau_{\mathrm{c}}} \tag{5.19}$$

where $V_{\mathrm{cmd}}(t)$ is the desired command potential, V is the actual membrane potential, τ_{c} is a time constant dependent on the series resistance, membrane capacitance and amount of compensation, and t_0 is a remaining, unexplained latency. The quality of fit is shown in the right panel of Fig. 5.9.

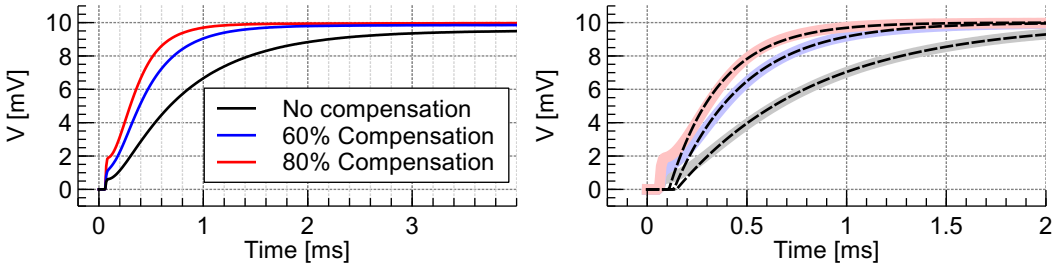

Figure 5.9: (Left) Membrane charging behavior measured in a model cell, during 'patch-clamp experiments' with 0%, 60% and 80% compensation. (Right) The charging behavior of a model cell can be modeled as an exponential convergence to the command potential and a slight delay. The thick, shadowed lines are the original traces from the left panel, the thin dashed lines are the fitted curves.

We found $\tau_{\mathrm{c}} \approx 0.70$ms uncompensated, $\tau_{\mathrm{c}} \approx 0.35$ms with 60% compensation and $\tau_{\mathrm{c}} \approx 0.26$ms with 80% compensation. By comparison, the values given by Beeler and Reuter's model for I_{Na} at -20mV are $\tau_m \approx 0.032$ms, $\tau_h \approx 1.1$ms and $\tau_j \approx 4.3$ms. This indicates that, even with good compensation, membrane charging will strongly interfere with the activation process, making τ_m more difficult to identify. With 'prediction' enabled (Sherman-Gold and Maertz, 2012), the situation is slightly more complex, as is shown in Fig. 5.10. However, for moderate prediction, the charging process is still reasonably well approximated by an exponential charging curve.

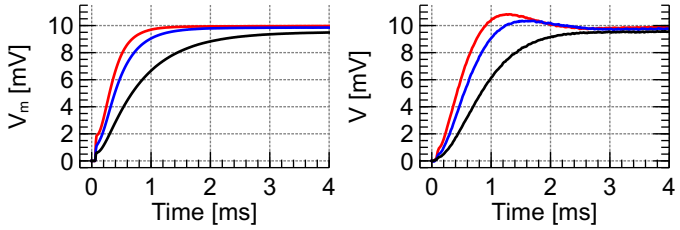

Figure 5.10: Uncompensated membrane charging (black) and charging with moderate (blue) or strong (red) compensation (left) or compensation/prediction (right).

To estimate the effects of membrane charging on I_{Na}, we updated our model of I_{Na} to include

a slowly charging membrane with $\tau_c \approx 0.3$ms. To reduce the number of extra parameters, the small latency t_0 seen in the model cell experiments was not included in the updated model. Because τ_c is not voltage-dependent we treated it as a single-valued parameter to be determined by the fitting procedure, and added it to the parameter vector p. With this updated model, we could simulate the effects of the membrane charging time on the fast sodium current. This is shown in Fig. 5.11 (left panel), which was made using the default model parameters given by Beeler and Reuter (for similar experiments using real cells, see Sherman et al., 1999). In the right panel, we show the ideal trace (i.e., with an instantaneously changing V) with a small time delay. This shows that the decaying part of the current is relatively unaffected by the slow membrane charging. By contrast, the time-to-peak, initial downward slope and peak current are all strongly affected.

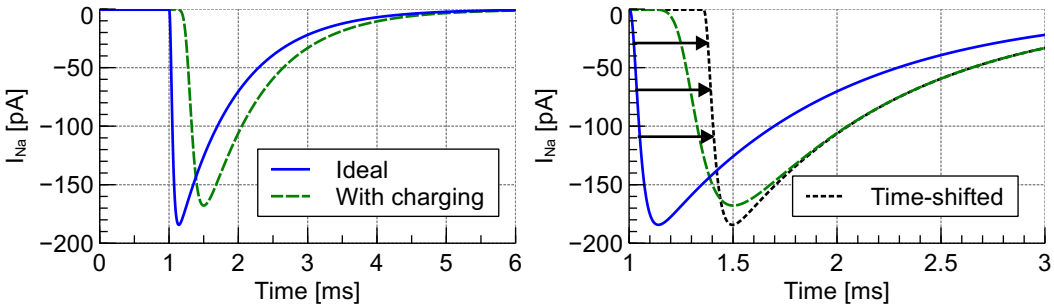

Figure 5.11: (Left) Simulated I_{Na} with ideal, instantaneous changes in membrane potential (blue, solid line) and with a realistic, series resistance compensated charging time (green, dashed). The charging time affects both the timing and the size of the peak. (Right) Time-shifting the ideal trace to overlap with the realistic trace reveals that the decaying phase is delayed, but otherwise unchanged (black dotted line).

The membrane charging time is not just an experimental issue, it also changes the identifiability of the model, making it more complex than the situation analyzed by Walch and Eisenberg. In their analysis, a single voltage step is considered so that V is piecewise constant, and the steady-state values and time constants for each V are single-valued parameters. Different step potentials V can then be applied and the appropriate constants worked out separately for each potential. Taking membrane charging time into account means adding a new variable to the model, but also means that, to accurately simulate a step from -120mV to -20mV, all values of the time constants and steady state values between -120mV and -20mV need to be identified simultaneously. However, provided the membrane charging time is short enough, only the activation process should be affected by this issue, as can be seen in the right panel of Fig. 5.11. To accommodate the changing V during activation, we used the full voltage-dependent parameters when fitting the model, allowing it to match the start of the experimental recording, even if in a non-unique way. Once the membrane is charged, the potential can once again be regarded as fixed. Based on the foregoing simulations and analysis we hypothesized that it should still be possible to

find reasonably accurate values for the time constants of inactivation. Similarly, the inaccuracy of dropping t_0 and not modeling the compensation/prediction curve will not affect inactivation measurements as long as the initial delay can be accommodated.

5.A.3 Repeated-fit experiments confirm our analysis

The top panel of Fig. 5.12 shows the variability observed between cells (i.e., single fits to different cells). It shows low variability in the steady-state values, but high variability for all time constants. The lower panel shows a similar graph for the variability observed between repeated fits to the same data from a representative cell ('cell 2'). Here it can be seen that, for the time constant of activation, the variability between repeated fits is similar to that observed between cells, so that no strong claims about inter-cell variability in activation can be made. Similarly, the variability observed in the determined steady-states can be explained as experimental error alone. By contrast, for the time constants of inactivation the variability between repeated fits is much lower than the inter-cell variability.

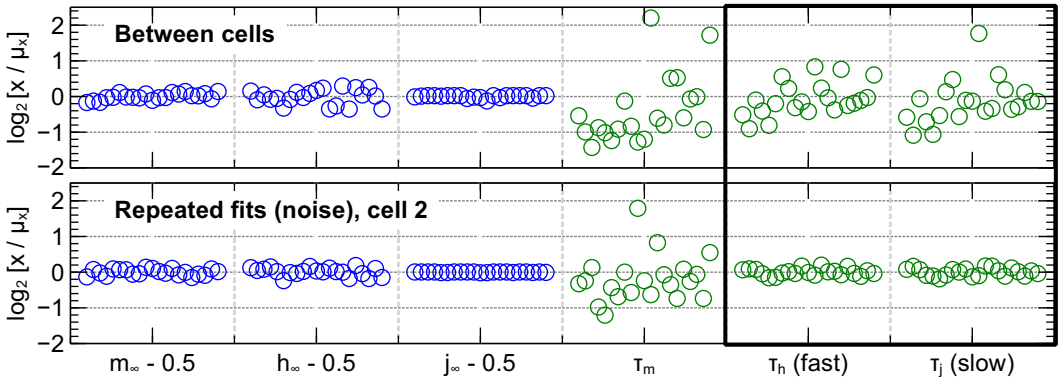

Figure 5.12: (*Top*) The variability in the parameters obtained by fitting our model to each of the 23 cells. For each parameter we show the $\log_2$ of its distance from the mean. The steady state parameters (m_∞, h_∞ and j_∞) were shifted by 0.5 to avoid dividing by zero, since $h_\infty \approx j_\infty \approx 0$. (*Bottom*) Variability in the parameters obtained by repeatedly fitting our model to the data from a single recording in cell 2 (data is shown from 23 re-runs).

5.B Additional results

5.B.1 Time-constant experiments

Fig. 5.13 shows alternative views of the I_{Na} measurements from Fig. 5.2. As can be seen, the maximum conductance varies widely, due to cell size, transfection success rate and differences in the kinetics of I_{Na} (as evinced by the different shapes of the curves, which are not simple linear multiples of each other).

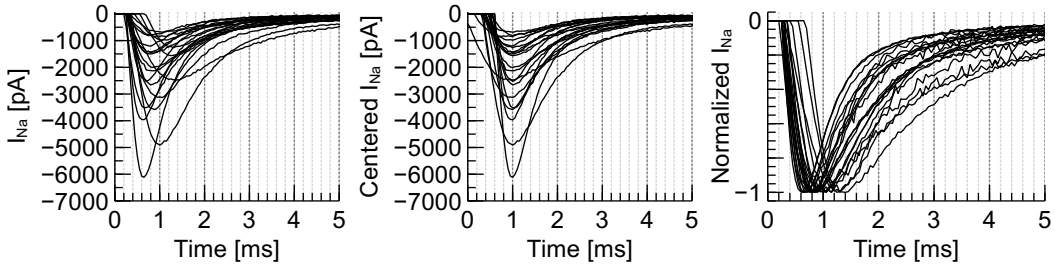

Figure 5.13: Alternative views of the single voltage-step experiments. (*Left*) The (pre-processed) data, without time-shifting or normalization. (*Middle*) The same data, time-shifted so that each peak occurs at $t = 1$ms. (*Right*) The same data, normalized to a peak-height of 1, without time-shifting.

Fig. 5.14 shows an example of the quality of fit obtained with the model including charging time.

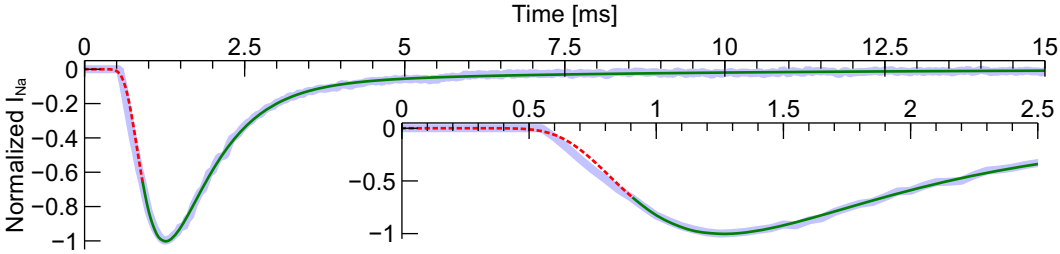

Figure 5.14: An example of the quality of fit obtained with the model including charging time. The raw data is shown in shaded blue. The model fit is shown as the solid green line. The dashed red lines indicates the part of the simulation that was not taken into account when calculating the score function. The inset gives a closer view of the same data during the initial downslope.

For 15 cells, we had two recordings made with a protocol containing a step from −120mV to −20mV. Fig. 5.15 shows the mean time constant determined using repeated fits to the recording from the first and second protocol for each of these cells. As can be seen, with a few exceptions, the cell behavior stayed constant during the experiment. Where values do vary, the direction of the change differs from cell to cell. This is inconsistent with the idea of

a slowly changing membrane potential due to flow of charged particles between the pipette and the cell, which would result in changes of a similar sign. On the basis of this figure, we also considered discarding the three cells that appear as 'outliers' in the top left of the left panel. However, the recordings showed no obvious deficiencies in leak or access resistance so that no objective criterion for rejecting them could be found. Removing these cells had a negligible effect on the corrected inter-cell standard deviations given in Section 5.3.1.3.

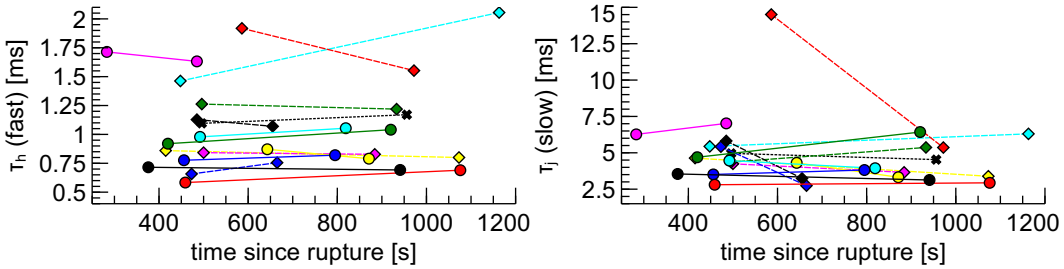

Figure 5.15: Changes in the time constants (determined as the mean constant using repeated fits) over time in 15 cells. Two time points are shown for each cell, connected by a line. Colors and markers are consistent between the left panel (fast inactivation) and the right (slow inactivation).

5.B.2 Midpoints of (in)activation in the biggest subgroup

Fig. 5.16.A shows the correlation between midpoint of activation and midpoint of inactivation for experiments in the largest subgroup. Regression coefficients were very similar to those found in the full dataset, with a slope of 1.13mV/mV and an offset of −38.3mV. The figure contains 28 points and has a slightly higher Pearson correlation coefficient than the full dataset (R=0.89). A distribution similar to Fig. 5.5.D but for the largest subgroup is shown in Fig. 5.16.B. Although there are fewer data points in these figures, the overall pattern is very similar.

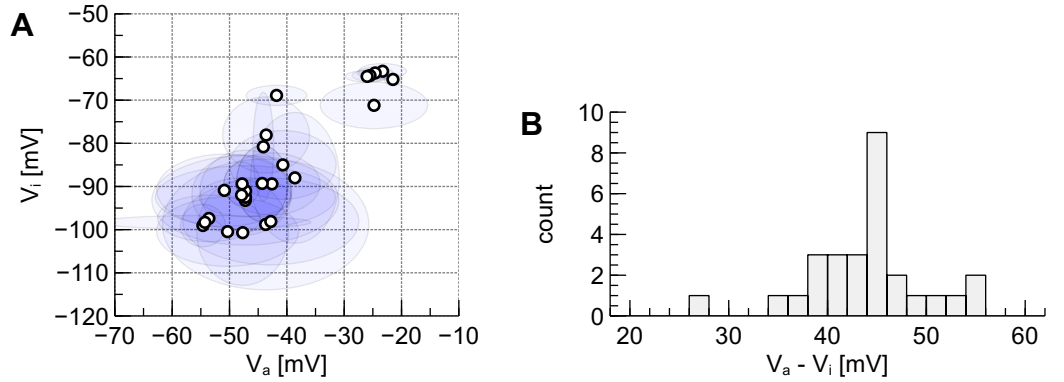

Figure 5.16: (*A*) Correlation between V_a and V_i in the largest subgroup. White dots indicate mean midpoints, blue ellipses indicate the corresponding $\pm 2\sigma$ range (*B*) A histogram of $V_a - V_i$ in the biggest subgroup.

5.B.3 β1-subunit coexpression

Table 5.4 shows the results from studies measuring midpoints of (in)activation of I_{Na} with and without β1-subunit. The table shows a variety of signs and magnitudes of reported shifts.

Table 5.4: Studies reporting midpoint of activation or inactivation with and without β1-subunit.

Midpoint of:	Activation [mV]			Inactivation [mV]				
	-β1	+β1	Shift	-β1	+β1	Shift	α	Cell type
An et al. (1998)				-70.2	-58.7	+11.5	a*	HEK
Bezzina et al. (2003)	-35.2	-39.9	-4.7	-78.3	-85.2	-6.9	a*	Oocyte
Calloe et al. (2011)	-34.4	-31.4	+3.0	-71.2	-77.7	-6.5	b	CHO
Groenewegen et al. (2003b)	-40.6	-38.63	+1.97	-82.75	-75	+7.75	a*	Oocyte
Wei et al. (1999)				-74.1	-63.2	+10.9	a*	Oocyte
Wan et al. (2000)	-33.4	-33.8	-0.4	-84.8	-79.3	+5.5	b*	Oocyte

5.C Studies used in the literature review

Table 5.5 shows all midpoints of (in)activation used in this study, along with the standard deviation (σ), number of cells (n) and the cell-type, α-subunit, and presence of β-subunit.

Table 5.5: Midpoints of (in)activation

Publication	V_a	σ_a	n_a	V_i	σ_i	n_i	Cell	α	β1
Abe et al. (2014)	-50.5	5.81	15	-84.1	5.03	15	HEK	b	no
Abriel et al. (2000)				-66.2	1.8	4	HEK	a*	yes
Abriel et al. (2001)	-21.5	0.735	6	-65.2	0.721	13	HEK	a*	yes
Abriel et al. (2001)	-23.3	2.08	3	-63.3	0.894	5	HEK	a*	yes
Abriel et al. (2001)	-24.6	1.56	3	-63.7	0.671	5	HEK	a*	yes
Abriel et al. (2001)	-25.5	1.56	3	-64.3	0.671	5	HEK	a*	yes
Abriel et al. (2001)	-26	1.91	3	-64.5	0.671	5	HEK	a*	yes
Aiba et al. (2014)	-43.3	4.76	7	-80.1	4.8	9	HEK	?	yes
Akai et al. (2000)	-44.1	0.9	9	-80.8	6.3	9	HEK	a*	yes
Albert et al. (2008)	-28.5	1.5	9	-60.8	0.959	23	Ooc.	a*	yes
Amin et al. (2005)	-36.7	6.96	10	-83.3	5.69	10	HEK	?	yes
An et al. (1998)				-70.2	5.36	17	HEK	a*	no
An et al. (1998)				-58.7	4.8	16	HEK	a*	yes
Bankston et al. (2007a)	-24.9	1.9	7	-61.3	3.67	5	HEK	?	yes
Bankston et al. (2007b)	-24.8	4.69	13	-71.2	2.7	9	HEK	a*	yes
Baroudi et al. (2000)				-101	5.63	22	HEK	a*	no
Baroudi et al. (2000)				-67.9	1.7	8	Ooc.	a*	no
Baroudi and Chahine (2000)	-47.2	8.15	23	-93.2	5.18	21	HEK	a*	yes
Baroudi et al. (2001)	-47.2	4.02	5	-92.5	2.26	4	HEK	a*	yes
Bébarová et al. (2008)	-31.8	4.8	16	-66.6	3.1	15	CHO	a	no
Beckermann et al. (2014)	-37.3	2.24	14	-86	1.33	11	HEK	?	yes
Beyder et al. (2010)	-33	22	6				HEK	b	no
Beyder et al. (2014)	-58.2	3	9	-95.5	3.9	9	HEK	b	no
Bezzina et al. (2003)	-35.2	14.7	8	-78.3	13	8	Ooc.	a*	no

Publication	V_a	σ_a	n_a	V_i	σ_i	n_i	Cell	α	$\beta 1$
Bezzina et al. (2003)	-39.9	8.6	4	-85.2	7.6	4	Ooc.	a*	yes
Calloe et al. (2011)	-34.4	0.566	8	-71.2	0.9	9	CHO	b	no
Calloe et al. (2011)	-31.4	1.26	10	-77.7	1.8	9	CHO	b	yes
Calloe et al. (2013)	-32.7	0.529	7	-69.5	0.529	7	CHO	b	no
Casini et al. (2007)	-38.6	3.87	15	-88	7.57	13	HEK	a*	yes
Chang et al. (2004)	-58.4	4.8	9	-107	2.7	9	HEK	?	yes
Chen et al. (2016)	-45.7	2.62	14	-80.7	4.5	12	HEK	?	yes
Cheng et al. (2010)	-32.2	3.2	16	-79.7	3.71	17	HEK	b	no
Cheng et al. (2010)	-31.1	3.43	6	-70.6	3.11	8	HEK	a	no
Cheng et al. (2010)	-34.9	3.6	9	-72	2.65	11	HEK	b	no
Cheng et al. (2010)	-34.9	2.01	5	-72.9	2.65	7	HEK	a	no
Cheng et al. (2011)	-37.6	3.39	8	-76.1	4.5	7	HEK	b	no
Cheng et al. (2011)	-39.6	5.59	5	-74.6	4.23	7	HEK	a	no
Clatot et al. (2012)	-44.3	6.6	17	-81.7	1.9	10	HEK	b*	no
Cordeiro et al. (2006)	-49.3	1.05	15	-93	0.538	10	HEK	b*	yes
Crotti et al. (2012)	-50.8	10.3	33	-92.5	4.21	17	HEK	?	yes
Deschênes et al. (2000)	-53.6	4.47	5	-97.4	2.69	6	HEK	a*	yes
Detta et al. (2014)	-40.3	1.53	11				HEK	a*	yes
Ellinor et al. (2008)	-21.2	2.32	15	-61.8	0.825	17	Ooc.	a*	yes
Ge et al. (2008)	-35.5	5.05	13	-78.7	6.63	26	HEK	a	yes
Glaaser et al. (2012)				-69.1	9.9	9	HEK	?	no
Gosselin-Badaroudine et al. (2012)	-55.3	2.28	7	-100	2.04	7	Ooc.	b	yes
Groenewegen et al. (2003b)	-40.6	6.08	15	-82.8	6.62	15	Ooc.	a*	no
Groenewegen et al. (2003b)	-38.6	8.77	8	-75	6.36	8	Ooc.	a*	yes
Groenewegen et al. (2003a)	-37.3	6.22	8	-78	4.05	7	Ooc.	a*	no
Gütter et al. (2013)	-35.1	3.75	88	-84.3	4.95	68	HEK	a*	no
Gütter et al. (2013)	-33.5	3.62	82	-71.2	3.7	28	Ooc.	a*	no
Gui et al. (2010a)	-34.7	3.36	23	-81.4	3.43	24	HEK	a*	no
Gui et al. (2010a)	-34.2	2.81	22	-67.7	2.78	31	Ooc.	a*	no
Gui et al. (2010b)	-33.8	2.32	11	-80.3	3.12	12	HEK	a*	no
Hayashi et al. (2015)	-43.8	6.8	16	-80	2.4	16	CHO	?	yes
Holst et al. (2009)	-30.4	2.24	14	-82	4.69	13	HEK	?	no
Hoshi et al. (2014)				-79.5	2.55	18	HEK	a	no
Hsueh et al. (2009)	-42.6	2.56	10	-84.3	3.79	10	HEK	a	yes
Hu et al. (2007)	-50.8	1.03	33	-92.5	0.412	17	HEK	b*	yes
Hu et al. (2010)				-92.5	4.21	17	HEK	?	yes
Hu et al. (2014)				-92.5	3.85	22	HEK	b	yes
Hu et al. (2015)	-41	3.9	9	-80	6.97	19	HEK	b	no
Hu et al. (2015)	-41	8.65	13	-80	9.35	14	HEK	a	no
Huang et al. (2006)	-59.9	2.55	8	-108	5.09	8	HEK	?	no
Huang et al. (2009)	-50.3	6.18	9	-100	4.02	9	HEK	a*	yes
Itoh et al. (2005a)	-39.9	7.5	25				HEK	a*	yes
Itoh et al. (2005b)	-40.6	6.42	21				HEK	a*	yes
Itoh et al. (2007)				-90.9	3.3	9	HEK	a*	yes
Juang et al. (2014)	-36.3	0.4	4	-86.4	1.4	4	HEK	a	yes
Kato et al. (2014)	-54.4	8.91	18	-83.8	9.62	21	CHO	a*	yes
Keller et al. (2005)	-41	6.9	9	-77.1	3.58	5	HEK	b*	yes
Keller et al. (2006)	-60.1	4.49	10	-104	1.81	8	HEK	?	yes
Li et al. (2009)	-56.6	4.21	6	-104	3.87	6	HEK	?	no

Publication	V_a	σ_a	n_a	V_i	σ_i	n_i	Cell	α	$\beta 1$
Lin et al. (2008)	-54.6	1.96	7	-99	2.46	8	HEK	a*	yes
Liu et al. (2002)				-73.3	6.2	4	HEK	a*	yes
Liu et al. (2003)	-50.4	4.38	11	-76.4	4.8	16	HEK	?	no
Liu et al. (2005)				-97	4.2	9	CHO	b	no
Lupoglazoff et al. (2001)	-47.2	7.85	19	-92.5	3.65	11	HEK	a*	yes
Makita et al. (1998)				-68.7	4.31	11	Ooc.	a*	no
Makita et al. (2002)	-47.2	3.97	13	-91	4.69	13	HEK	a*	yes
Makita et al. (2005)	-48.1	3.92	19	-86.6	3.71	17	HEK	?	yes
Makita et al. (2008)	-49.7	6.22	32	-86.8	5.5	25	HEK	?	yes
Makiyama et al. (2008)	-43.6	3.79	23	-78.1	4.41	22	HEK	a*	yes
Marangoni et al. (2011)	-44	8	16	-92	7.21	13	HEK	?	yes
Medeiros-Domingo et al. (2007)	-43.8	2.86	5	-78.8	3.51	10	HEK	?	no
Medeiros-Domingo et al. (2009)	-38.6	3.49	15	-76	5.23	19	HEK	b	no
Mohler et al. (2004)	-41.8	2.65	7	-68.9	1.16	15	HEK	a*	yes
Mok et al. (2003)	-47.2	5.6	4	-91.1	0.693	3	HEK	?	yes
Moreau et al. (2013)	-47.9	4.33	13	-92	4.69	13	HEK	a*	yes
Murphy et al. (2012)	-50.9	10.3	20	-102	6.32	10	HEK	a*	no
Nakajima et al. (2015)	-38.7	3.1	15	-85.9	2.47	17	HEK	b	yes
Neu et al. (2010)	-50.9	5.89	12	-90.9	4.2	9	HEK	a*	yes
Nguyen et al. (2008)	-47.8	1.58	10	-89.4	2.53	10	HEK	a*	yes
O'Leary et al. (2002)				-78.6	0.134	5	Ooc.	?	no
Olesen et al. (2012)	-27.9	6.1	22	-85.6	4.5	25	HEK	?	no
Otagiri et al. (2008)	-44.4	4.26	37	-88.3	4.87	37	HEK	?	yes
Pfahnl et al. (2007)	-50	1.55	15	-98	8.52	15	HEK	b*	no
Poelzing et al. (2006)							HEK	a	no
Rivolta et al. (2001)	-23.3	2.24	5	-62.8	3.12	12	HEK	?	yes
Rook et al. (1999)	-35.9	0.949	10	-77.4	0.316	10	Ooc.	a*	no
Rossenbacker et al. (2004)	-24.1	0.894	5	-70.9	1.4	4	HEK	?	yes
Ruan et al. (2007)	-23.2	1.92	5	-62.5	2.15	10	HEK	?	yes
Ruan et al. (2010)	-23.1	1.77	9	-67.7	3.01	12	HEK	?	yes
Saber et al. (2015)	-24	4.9	6	-66	4.9	6	HEK	?	yes
Samani et al. (2009)	-36	5.03	7	-89.9	5.4	9	HEK	b	yes
Sarhan et al. (2009)				-109	1.85	7	HEK	a	no
Shinlapawittayatorn et al. (2011b)				-91.9	4.5	7	HEK	a	no
Shinlapawittayatorn et al. (2011a)				-91.2	2.77	12	HEK	a	no
Shirai et al. (2002)	-49.9	2.38	7	-94.9	6.37	6	HEK	a*	no
Shuraih et al. (2007)	-43.4	0.794	7	-90.7	0.265	7	HEK	b	yes
Shy et al. (2014)	-29.6	3.68	8	-76.9	6.96	10	HEK	?	no
Smits et al. (2005a)	-42.6	4.2	9	-89.4	3.6	9	HEK	a*	yes
Smits et al. (2005b)	-43.7	9	9	-98.8	7.57	13	HEK	a*	yes
Sottas et al. (2013)	-29.8	1.99	11	-72.2	1.66	11	HEK	?	yes
Splawski et al. (2002)	-26.6	3.68	8				HEK	?	no
Surber et al. (2008)	-31.5	7.27	27	-67.6	3.7	28	Ooc.	a*	no
Surber et al. (2008)	-42.2	3.37	14	-79.4	3.43	6	HEK	a*	no
Swan et al. (2014)	-28	3.39	8	-75.8	4.9	6	HEK	b	yes
Tan et al. (2001)	-48.6	3.17	7	-92	4.5	7	HEK	?	yes
Tan et al. (2002)	-40.3	2.88	13	-93.5	4.33	13	HEK	a*	no
Tan et al. (2005)	-39	4.9	6	-75	5.66	8	HEK	b	no
Tan et al. (2005)	-38	4.9	6	-75	6	9	HEK	b	no

Publication	V_a	σ_a	n_a	V_i	σ_i	n_i	Cell	α	$\beta 1$
Tan et al. (2005)	-42	2.91	5	-81	4.2	9	HEK	b	no
Tan et al. (2005)	-41	3.39	8	-79	5.31	11	HEK	b	no
Tan et al. (2005)	-42	2.55	8	-79	4.2	9	HEK	b	no
Tan et al. (2005)	-40	9.55	6	-78	7.83	5	HEK	b	no
Tan et al. (2005)	-40	1.39	3	-81	4.68	3	HEK	b	no
Tan et al. (2005)	-39	4	4	-75	5.66	8	HEK	a	no
Tan et al. (2005)	-39	4	4	-78	2.83	8	HEK	a	no
Tan et al. (2005)	-42	3.96	8	-82	4.85	12	HEK	a	no
Tan et al. (2005)	-40	8.49	18	-79	8.49	18	HEK	a	no
Tan et al. (2005)	-43	2	4	-82	6.2	4	HEK	a	no
Tan et al. (2005)	-42	3.39	8	-82	3.6	9	HEK	a	no
Tan et al. (2005)	-40	5.66	8	-80	4.8	9	HEK	a	no
Tan et al. (2005)	-41	1.8	4	-80	1.2	4	HEK	a	no
Tan et al. (2006)	-46.9	3.39	8	-81.8	3.68	8	HEK	b	no
Tan et al. (2006)	-44.1	5.06	10	-80	4.74	10	HEK	a	no
Tarradas et al. (2013)	-32	1.27	18	-84.9	2.85	10	HEK	a*	no
Tester et al. (2010)	-42	4	4	-72	2.24	5	HEK	b	no
Tsurugi et al. (2009)	-39.6	3.39	8	-88	2.55	8	HEK	?	no
Valdivia et al. (2004)	-42	7.75	15	-84.3	4.47	20	HEK	b	no
Vatta et al. (2002a)				-89.5	0.49	6	HEK	?	no
Vatta et al. (2002b)	-24.9	1.13	8	-68.4	0.332	11	Ooc.	?	no
Viswanathan et al. (2003)	-40.7	4.64	11	-85	3.98	11	HEK	a*	yes
Wang et al. (1996)	-43.2	6.85	13	-99.6	2.92	11	HEK	a*	no
Wang et al. (2002)	-47.7	4	16	-101	6.1	19	HEK	a*	yes
Wang et al. (2007a)	-44.3	2.24	14	-89.3	4.4	16	HEK	a*	yes
Wang et al. (2007b)	-46	6.93	5				HEK	a*	yes
Wang et al. (2008)	-44.3	2.24	14	-89.3	4.4	16	HEK	a*	yes
Wang et al. (2011)				-93.9	2.65	11	HEK	?	no
Wang et al. (2015)	-40.9	0.63	9	-72.7	2.49	7	HEK	a*	no
Wang et al. (2016)	-44.5	4.8	36	-93.5	4.08	34	HEK	?	yes
Watanabe et al. (2011b)	-35.4	3	25	-84.5	4.9	24	CHO	a	no
Watanabe et al. (2011b)	-47.7	4.4	16	-89.4	3.05	19	HEK	a	no
Wedekind et al. (2001)	-42.8	7.67	7	-98.1	5.03	7	HEK	a*	yes
Wehrens et al. (2003)	-29.8	1.13	8	-64	2.26	8	HEK	?	yes
Wei et al. (1999)				-63.2	4.11	10	Ooc.	a*	yes
Wei et al. (1999)				-74.1	2.38	7	Ooc.	a*	no
Winkel et al. (2012)	-26	10.3	17	-84.6	7.2	16	HEK	?	no
Yang et al. (2002)	-54.3	9.26	7	-98.3	0.794	7	HEK	a*	yes
Ye et al. (2003)	-44	15.8	10	-95	14.4	9	HEK	a*	no
Ye et al. (2003)	-40	18.5	7	-86	15.3	7	HEK	b*	no
Yokoi et al. (2005)	-49.8	3.68	8	-88.6	3	9	HEK	?	no
Young and Caldwell (2005)	-32.7	5.81	20	-66	8.94	20	CHO	a*	no
Zeng et al. (2013)	-34.5	4.24	8	-81.1	4.69	13	HEK	a	yes
Zhang et al. (2008)	-33.1	2.24	5	-64.5	0.98	6	Ooc.	a*	no
Zhang et al. (2015)	-28.1	5.03	15				HEK	?	no

References

Abe, K., Machida, T., Sumitomo, N., Yamamoto, H., Ohkubo, K., Watanabe, I., Makiyama, T., Fukae, S., Kohno, M., Harrell, D.T., et al., 2014. Sodium channelopathy underlying familial sick sinus syndrome with early onset and predominantly male characteristics. Circulation: Arrhythmia and Electrophysiology 7, 511–517.

Abriel, H., Cabo, C., Wehrens, X.H., Rivolta, I., Motoike, H.K., Memmi, M., Napolitano, C., Priori, S.G., Kass, R.S., 2001. Novel arrhythmogenic mechanism revealed by a long-QT syndrome mutation in the cardiac Na+ channel. Circulation Research 88, 740–745.

Abriel, H., De Lange, E., Kucera, J.P., Loussouarn, G., Tarek, M., 2013. Computational tools to investigate genetic cardiac channelopathies. Frontiers in Physiology 4, 390.

Abriel, H., Wehrens, X., Benhorin, J., Kerem, B., Kass, R., 2000. Molecular pharmacology of the sodium channel mutation D1790G linked to the long-QT syndrome. Circulation 102, 921–925.

Aiba, T., Farinelli, F., Kostecki, G., Hesketh, G.G., Edwards, D., Biswas, S., Tung, L., Tomaselli, G.F., 2014. A mutation causing Brugada syndrome identifies a mechanism for altered autonomic and oxidant regulation of cardiac sodium currents. Circulation: Cardiovascular Genetics 7, 249–256.

Akai, J., Makita, N., Sakurada, H., Shirai, N., Ueda, K., Kitabatake, A., Nakazawa, K., Kimura, A., Hiraoka, M., 2000. A novel SCN5A mutation associated with idiopathic ventricular fibrillation without typical ECG findings of Brugada syndrome. FEBS Letters 479, 29–34.

Albert, C.M., Nam, E.G., Rimm, E.B., Jin, H.W., Hajjar, R.J., Hunter, D.J., MacRae, C.A., Ellinor, P.T., 2008. Cardiac sodium channel gene variants and sudden cardiac death in women. Circulation 117, 16–23.

Amin, A., Verkerk, A., Bhuiyan, Z., Wilde, A., Tan, H., 2005. Novel Brugada syndrome-causing mutation in ion-conducting pore of cardiac Na+ channel does not affect ion selectivity properties. Acta Physiologica Scandinavica 185, 291–301.

Amin, A.S., Asghari-Roodsari, A., Tan, H.L., 2010. Cardiac sodium channelopathies. Pflügers Archiv-European Journal of Physiology 460, 223–237.

An, R., Wang, X., Kerem, B., Benhorin, J., Medina, A., Goldmit, M., Kass, R., 1998. Novel LQT-3 mutation affects Na+ channel activity through interactions between α-and β1-subunits. Circulation Research 83, 141–146.

Bankston, J.R., Sampson, K.J., Kateriya, S., Glaaser, I.W., Malito, D.L., Chung, W.K., Kass, R.S., 2007a. A novel LQT-3 mutation disrupts an inactivation gate complex with distinct rate-dependent phenotypic consequences. Channels 1, 273–280.

Bankston, J.R., Yue, M., Chung, W., Spyres, M., Pass, R.H., Silver, E., Sampson, K.J., Kass,

R.S., 2007b. A novel and lethal de novo LQT-3 mutation in a newborn with distinct molecular pharmacology and therapeutic response. PLOS ONE 2, e1258.

Baroudi, G., Carbonneau, E., Pouliot, V., Chahine, M., 2000. SCN5A mutation (T1620M) causing Brugada syndrome exhibits different phenotypes when expressed in Xenopus oocytes and mammalian cells. FEBS Letters 467, 12–16.

Baroudi, G., Chahine, M., 2000. Biophysical phenotypes of SCN5A mutations causing long QT and Brugada syndromes. FEBS Letters 487, 224–228.

Baroudi, G., Pouliot, V., Denjoy, I., Guicheney, P., Shrier, A., Chahine, M., 2001. Novel mechanism for Brugada syndrome defective surface localization of an SCN5A mutant (R1432G). Circulation Research 88, e78–e83.

Bébarová, M., O'Hara, T., Geelen, J.L., Jongbloed, R.J., Timmermans, C., Arens, Y.H., Rodriguez, L.M., Rudy, Y., Volders, P.G., 2008. Subepicardial phase 0 block and discontinuous transmural conduction underlie right precordial ST-segment elevation by a SCN5A loss-of-function mutation. American Journal of Physiology – Heart and Circulatory Physiology 295, H48–H58.

Beckermann, T.M., McLeod, K., Murday, V., Potet, F., George, A.L., 2014. Novel SCN5A mutation in amiodarone-responsive multifocal ventricular ectopy-associated cardiomyopathy. Heart Rhythm 11, 1446–1453.

Beeler, G.W., Reuter, H., 1977. Reconstruction of the action potential of ventricular myocardial fibres. The Journal of Physiology 268, 177–210.

Beyder, A., Mazzone, A., Strege, P.R., Tester, D.J., Saito, Y.A., Bernard, C.E., Enders, F.T., Ek, W.E., Schmidt, P.T., Dlugosz, A., et al., 2014. Loss-of-function of the voltage-gated sodium channel NaV1.5 (channelopathies) in patients with irritable bowel syndrome. Gastroenterology 146, 1659–1668.

Beyder, A., Rae, J.L., Bernard, C., Strege, P.R., Sachs, F., Farrugia, G., 2010. Mechanosensitivity of NaV1.5, a voltage-sensitive sodium channel. The Journal of Physiology 588, 4969–4985.

Bezzina, C.R., Rook, M.B., Groenewegen, W.A., Herfst, L.J., van der Wal, A.C., Lam, J., Jongsma, H.J., Wilde, A.A., Mannens, M.M., 2003. Compound heterozygosity for mutations (W156X and R225W) in SCN5A associated with severe cardiac conduction disturbances and degenerative changes in the conduction system. Circulation Research 92, 159–168.

Britton, O.J., Bueno-Orovio, A., Van Ammel, K., Lu, H.R., Towart, R., Gallacher, D.J., Rodriguez, B., 2013. Experimentally calibrated population of models predicts and explains intersubject variability in cardiac cellular electrophysiology. Proceedings of the National Academy of Sciences 110, E2098–E2105.

Calloe, K., Refaat, M.M., Grubb, S., Wojciak, J., Campagna, J., Thomsen, N.M., Nussbaum, R.L., Scheinman, M.M., Schmitt, N., 2013. Characterization and mechanisms of action of novel NaV1.5 channel mutations associated with Brugada syndrome. Circulation: Arrhythmia and Electrophysiology 6, 177–184.

Calloe, K., Schmitt, N., Grubb, S., Pfeiffer, R., David, J.P., Kanter, R., Cordeiro, J.M., Antzelevitch, C., 2011. Multiple arrhythmic syndromes in a newborn, owing to a novel mutation in

SCN5A. Canadian Journal of Physiology and Pharmacology 89, 723–736.

Casini, S., Tan, H.L., Bhuiyan, Z.A., Bezzina, C.R., Barnett, P., Cerbai, E., Mugelli, A., Wilde, A.A., Veldkamp, M.W., 2007. Characterization of a novel SCN5A mutation associated with Brugada syndrome reveals involvement of DIIIS4–S5 linker in slow inactivation. Cardiovascular Research 76, 418–429.

Chang, C.C., Acharfi, S., Wu, M.H., Chiang, F.T., Wang, J.K., Sung, T.C., Chahine, M., 2004. A novel SCN5A mutation manifests as a malignant form of long QT syndrome with perinatal onset of tachycardia/bradycardia. Cardiovascular Research 64, 268–278.

Chang, E.T., Strong, M., Clayton, R.H., 2015. Bayesian sensitivity analysis of a cardiac cell model using a Gaussian process emulator. PLOS ONE 10, e0130252.

Chen, J., Makiyama, T., Wuriyanghai, Y., Ohno, S., Sasaki, K., Hayano, M., Harita, T., Nishiuchi, S., Yamamoto, Y., Ueyama, T., et al., 2016. Cardiac sodium channel mutation associated with epinephrine-induced QT prolongation and sinus node dysfunction. Heart Rhythm 13, 289–298.

Cheng, J., Morales, A., Siegfried, J.D., Li, D., Norton, N., Song, J., Gonzalez-Quintana, J., Makielski, J.C., Hershberger, R.E., 2010. SCN5A rare variants in familial dilated cardiomyopathy decrease peak sodium current depending on the common polymorphism H558R and common splice variant Q1077del. Clinical and Translational Science 3, 287–294.

Cheng, J., Tester, D.J., Tan, B.H., Valdivia, C.R., Kroboth, S., Ye, B., January, C.T., Ackerman, M.J., Makielski, J.C., 2011. The common African American polymorphism SCN5A-S1103Y interacts with mutation SCN5A-R680H to increase late Na current. Physiological Genomics 43, 461–466.

Clatot, J., Ziyadeh-Isleem, A., Maugenre, S., Denjoy, I., Liu, H., Dilanian, G., Hatem, S.N., Deschênes, I., Coulombe, A., Guicheney, P., et al., 2012. Dominant-negative effect of SCN5A N-terminal mutations through the interaction of NaV1.5 α-subunits. Cardiovascular Research 96, 53–63.

Clerx, M., Collins, P., Volders, P.G.A., 2015. Applying novel identification protocols to Markov models of INa, in: Computing in Cardiology, CINC. pp. 889–892.

Cordeiro, J.M., Barajas-Martinez, H., Hong, K., Burashnikov, E., Pfeiffer, R., Orsino, A.M., Wu, Y.S., Hu, D., Brugada, J., Brugada, P., et al., 2006. Compound heterozygous mutations P336L and I1660V in the human cardiac sodium channel associated with the Brugada syndrome. Circulation 114, 2026–2033.

Crotti, L., Hu, D., Barajas-Martinez, H., De Ferrari, G.M., Oliva, A., Insolia, R., Pollevick, G.D., Dagradi, F., Guerchicoff, A., Greco, F., et al., 2012. Torsades de pointes following acute myocardial infarction: evidence for a deadly link with a common genetic variant. Heart Rhythm 9, 1104–1112.

Deschênes, I., Baroudi, G., Berthet, M., Barde, I., Chalvidan, T., Denjoy, I., Guicheney, P., Chahine, M., 2000. Electrophysiological characterization of SCN5A mutations causing long QT (E1784K) and Brugada (R1512W and R1432G) syndromes. Cardiovascular Research 46, 55–65.

Detta, N., Frisso, G., Limongelli, G., Marzullo, M., Calabrò, R., Salvatore, F., 2014. Genetic

analysis in a family affected by sick sinus syndrome may reduce the sudden death risk in a young aspiring competitive athlete. International Journal of Cardiology 170, e63–e65.

Drummond, G., Vowler, S., 2011. Show the data, don't conceal them. The Journal of Physiology 589, 1861.

Eberhart, R.C., Kennedy, J., 1995. A new optimizer using particle swarm theory, in: Proceedings of the Sixth International Symposium on Micro Machine and Human Science, New York, NY. pp. 39–43.

Ellinor, P.T., Nam, E.G., Shea, M.A., Milan, D.J., Ruskin, J.N., MacRae, C.A., 2008. Cardiac sodium channel mutation in atrial fibrillation. Heart Rhythm 5, 99–105.

Feng, J., Li, G.r., Fermini, B., Nattel, S., 1996. Properties of sodium and potassium currents of cultured adult human atrial myocytes. American Journal of Physiology – Heart and Circulatory Physiology 270, H1676–H1686.

Fernandez, F.R., Morales, E., Rashid, A.J., Dunn, R.J., Turner, R.W., 2003. Inactivation of Kv3.3 potassium channels in heterologous expression systems. Journal of Biological Chemistry 278, 40890–40898.

Ge, J., Sun, A., Paajanen, V., Wang, S., Su, C., Yang, Z., Li, Y., Wang, S., Jia, J., Wang, K., et al., 2008. Molecular and clinical characterization of a novel SCN5A mutation associated with atrioventricular block and dilated cardiomyopathy. Circulation: Arrhythmia and Electrophysiology 1, 83–92.

Glaaser, I.W., Osteen, J.D., Puckerin, A., Sampson, K.J., Jin, X., Kass, R.S., 2012. Perturbation of sodium channel structure by an inherited long QT syndrome mutation. Nature Communications 3, 706.

Gosselin-Badaroudine, P., Keller, D.I., Huang, H., Pouliot, V., Chatelier, A., Osswald, S., Brink, M., Chahine, M., 2012. A proton leak current through the cardiac sodium channel is linked to mixed arrhythmia and the dilated cardiomyopathy phenotype. PLOS ONE 7, e38331.

Grandi, E., Pasqualini, F.S., Bers, D.M., 2010. A novel computational model of the human ventricular action potential and Ca transient. Journal of Molecular and Cellular Cardiology 48, 112–121.

Groenewegen, W.A., Bezzina, C.R., van Tintelen, J.P., Hoorntje, T.M., Mannens, M.M., Wilde, A.A., Jongsma, H.J., Rook, M.B., 2003a. A novel LQT3 mutation implicates the human cardiac sodium channel domain IVS6 in inactivation kinetics. Cardiovascular Research 57, 1072–1078.

Groenewegen, W.A., Firouzi, M., Bezzina, C.R., Vliex, S., van Langen, I.M., Sandkuijl, L., Smits, J.P., Hulsbeek, M., Rook, M.B., Jongsma, H.J., et al., 2003b. A cardiac sodium channel mutation cosegregates with a rare connexin 40 genotype in familial atrial standstill. Circulation Research 92, 14–22.

Gui, J., Wang, T., Jones, R.P., Trump, D., Zimmer, T., Lei, M., 2010a. Multiple loss-of-function mechanisms contribute to SCN5A-related familial sick sinus syndrome. PLOS ONE 5, e10985.

Gui, J., Wang, T., Trump, D., Zimmer, T., Lei, M., 2010b. Mutation-specific effects of polymorphism H558R in SCN5A-related sick sinus syndrome. Journal of Cardiovascular Electrophysiology

21, 564–573.

Gütter, C., Benndorf, K., Zimmer, T., 2013. Characterization of N-terminally mutated cardiac Na+ channels associated with long QT syndrome 3 and Brugada syndrome. Sudden arrhythmic death: from basic science to clinical practice , 41.

Hanck, D.A., Sheets, M.F., 1992. Time-dependent changes in kinetics of Na^+ current in single canine cardiac Purkinje cells. American Journal of Physiology – Heart and Circulatory Physiology 262, H1197–H1207.

Hayashi, K., Konno, T., Tada, H., Tani, S., Liu, L., Fujino, N., Nohara, A., Hodatsu, A., Tsuda, T., Tanaka, Y., et al., 2015. Functional characterization of rare variants implicated in susceptibility to lone atrial fibrillation. Circulation: Arrhythmia and Electrophysiology 8, 1095–1104.

Holst, A.G., Calloe, K., Jespersen, T., Cedergreen, P., Winkel, B.G., Jensen, H.K., Leren, T.P., Haunso, S., Svendsen, J.H., Tfelt-Hansen, J., 2009. A novel SCN5A mutation in a patient with coexistence of Brugada syndrome traits and ischaemic heart disease. Case Reports in Medicine 2009.

Hoshi, M., Du, X.X., Shinlapawittayatorn, K., Liu, H., Chai, S., Wan, X., Ficker, E., Deschênes, I., 2014. Brugada syndrome disease phenotype explained in apparently benign sodium channel mutations. Circulation: Cardiovascular Genetics 7, 123.

Hsueh, C.H., Chen, W.P., Lin, J.L., Tsai, C.T., Liu, Y.B., Juang, J.M., Tsao, H.M., Su, M.J., Lai, L.P., 2009. Distinct functional defect of three novel Brugada syndrome related cardiac sodium channel mutations. Journal of Biomedical Science 16, 1.

Hu, D., Barajas-Martinez, H., Nesterenko, V.V., Pfeiffer, R., Guerchicoff, A., Cordeiro, J.M., Curtis, A.B., Pollevick, G.D., Wu, Y., Burashnikov, E., et al., 2010. Dual variation in SCN5A and CACNB2b underlies the development of cardiac conduction disease without Brugada syndrome. Pacing and Clinical Electrophysiology 33, 274–285.

Hu, D., Barajas-Martínez, H., Terzic, A., Park, S., Pfeiffer, R., Burashnikov, E., Wu, Y., Borggrefe, M., Veltmann, C., Schimpf, R., et al., 2014. ABCC9 is a novel Brugada and early repolarization syndrome susceptibility gene. International Journal of Cardiology 171, 431–442.

Hu, D., Viskin, S., Oliva, A., Carrier, T., Cordeiro, J.M., Barajas-Martinez, H., Wu, Y., Burashnikov, E., Sicouri, S., Brugada, R., et al., 2007. Novel mutation in the SCN5A gene associated with arrhythmic storm development during acute myocardial infarction. Heart Rhythm 4, 1072–1080.

Hu, R.M., Tan, B.H., Tester, D.J., Song, C., He, Y., Dovat, S., Peterson, B.Z., Ackerman, M.J., Makielski, J.C., 2015. Arrhythmogenic biophysical phenotype for SCN5A mutation S1787N depends upon splice variant background and intracellular acidosis. PLOS ONE 10, e0124921.

Huang, H., Millat, G., Rodriguez-Lafrasse, C., Rousson, R., Kugener, B., Chevalier, P., Chahine, M., 2009. Biophysical characterization of a new SCN5A mutation S1333Y in a SIDS infant linked to long QT syndrome. FEBS Letters 583, 890–896.

Huang, H., Zhao, J., Barrane, F.Z., Champagne, J., Chahine, M., 2006. NaV1.5/R1193Q polymorphism is associated with both long QT and Brugada syndromes. Canadian Journal of Cardiology

22, 309–313.

Itoh, H., Shimizu, M., Mabuchi, H., Imoto, K., 2005a. Clinical and electrophysiological characteristics of Brugada syndrome caused by a missense mutation in the S5-pore site of SCN5A. Journal of Cardiovascular Electrophysiology 16, 378–383.

Itoh, H., Shimizu, M., Takata, S., Mabuchi, H., Imoto, K., 2005b. A novel missense mutation in the SCN5A gene associated with Brugada syndrome bidirectionally affecting blocking actions of antiarrhythmic drugs. Journal of Cardiovascular Electrophysiology 16, 486–493.

Itoh, H., Tsuji, K., Sakaguchi, T., Nagaoka, I., Oka, Y., Nakazawa, Y., Yao, T., Jo, H., Ashihara, T., Ito, M., et al., 2007. A paradoxical effect of lidocaine for the N406S mutation of SCN5A associated with Brugada syndrome. International Journal of Cardiology 121, 239–248.

Jones, E., Oliphant, T., Peterson, P., et al., 2001. SciPy: Open source scientific tools for Python. [Online; accessed 2015-01-14].

Juang, J.M.J., Lu, T.P., Lai, L.C., Hsueh, C.H., Liu, Y.B., Tsai, C.T., Lin, L.Y., Yu, C.C., Hwang, J.J., Chiang, F.T., et al., 2014. Utilizing multiple in silico analyses to identify putative causal SCN5A variants in Brugada syndrome. Scientific Reports 4, 3850.

Kato, K., Makiyama, T., Wu, J., Ding, W.G., Kimura, H., Naiki, N., Ohno, S., Itoh, H., Nakanishi, T., Matsuura, H., et al., 2014. Cardiac channelopathies associated with infantile fatal ventricular arrhythmias: from the cradle to the bench. Journal of Cardiovascular Electrophysiology 25, 66–73.

Keller, D.I., Huang, H., Zhao, J., Frank, R., Suarez, V., Delacrétaz, E., Brink, M., Osswald, S., Schwick, N., Chahine, M., 2006. A novel SCN5A mutation, F1344S, identified in a patient with Brugada syndrome and fever-induced ventricular fibrillation. Cardiovascular Research 70, 521–529.

Keller, D.I., Rougier, J.S., Kucera, J.P., Benammar, N., Fressart, V., Guicheney, P., Madle, A., Fromer, M., Schläpfer, J., Abriel, H., 2005. Brugada syndrome and fever: genetic and molecular characterization of patients carrying SCN5A mutations. Cardiovascular Research 67, 510–519.

Li, Q., Huang, H., Liu, G., Lam, K., Rutberg, J., Green, M.S., Birnie, D.H., Lemery, R., Chahine, M., Gollob, M.H., 2009. Gain-of-function mutation of NaV1.5 in atrial fibrillation enhances cellular excitability and lowers the threshold for action potential firing. Biochemical and Biophysical Research Communications 380, 132–137.

Lin, M.T., Wu, M.H., Chang, C.C., Chiu, S.N., Thériault, O., Huang, H., Christé, G., Ficker, E., Chahine, M., 2008. In utero onset of long QT syndrome with atrioventricular block and spontaneous or lidocaine-induced ventricular tachycardia: compound effects of hERG pore region mutation and SCN5A N-terminus variant. Heart Rhythm 5, 1567–1574.

Liu, C.j., Dib-Hajj, S.D., Renganathan, M., Cummins, T.R., Waxman, S.G., 2003. Modulation of the cardiac sodium channel NaV1.5 by fibroblast growth factor homologous factor 1B. Journal of Biological Chemistry 278, 1029–1036.

Liu, H., Tateyama, M., Clancy, C.E., Abriel, H., Kass, R.S., 2002. Channel openings are necessary but not sufficient for use-dependent block of cardiac Na+ channels by flecainide evidence from

the analysis of disease-linked mutations. The Journal of General Physiology 120, 39–51.

Liu, K., Yang, T., Viswanathan, P.C., Roden, D.M., 2005. New mechanism contributing to drug-induced arrhythmia rescue of a misprocessed LQT3 mutant. Circulation 112, 3239–3246.

Loewe, A., Wilhelms, M., Fischer, F., Scholz, E., Dössel, O., 2013. Impact of hERG mutations on simulated human atrial action potentials. Biomedical Engineering / Biomedizinische Technik 58.

Loewe, A., Wilhelms, M., Schmid, J., Krause, M.J., Fischer, F., Thomas, D., Scholz, E.P., Dössel, O., Seemann, G., 2016. Parameter estimation of ion current formulations requires hybrid optimization approach to be both accurate and reliable. Frontiers in Bioengineering and Biotechnology 3, 1–13.

Lupoglazoff, J., Cheav, T., Baroudi, G., Berthet, M., Denjoy, I., Cauchemez, B., Extramiana, F., Chahine, M., Guicheney, P., 2001. Homozygous SCN5A mutation in long-QT syndrome with functional two-to-one atrioventricular block. Circulation Research 89, e16–e21.

Makielski, J.C., Ye, B., Valdivia, C.R., Pagel, M.D., Pu, J., Tester, D.J., Ackerman, M.J., 2003. A ubiquitous splice variant and a common polymorphism affect heterologous expression of recombinant human SCN5A heart sodium channels. Circulation Research 93, 821–828.

Makita, N., Behr, E., Shimizu, W., Horie, M., Sunami, A., Crotti, L., Schulze-Bahr, E., Fukuhara, S., Mochizuki, N., Makiyama, T., et al., 2008. The E1784K mutation in SCN5A is associated with mixed clinical phenotype of type 3 long QT syndrome. The Journal of Clinical Investigation 118, 2219–2229.

Makita, N., Horie, M., Nakamura, T., Ai, T., Sasaki, K., Yokoi, H., Sakurai, M., Sakuma, I., Otani, H., Sawa, H., et al., 2002. Drug-induced long-QT syndrome associated with a subclinical SCN5A mutation. Circulation 106, 1269–1274.

Makita, N., Sasaki, K., Groenewegen, W.A., Yokota, T., Yokoshiki, H., Murakami, T., Tsutsui, H., 2005. Congenital atrial standstill associated with coinheritance of a novel SCN5A mutation and connexin 40 polymorphisms. Heart Rhythm 2, 1128–1134.

Makita, N., Shirai, N., Nagashima, M., Matsuoka, R., Yamada, Y., Tohse, N., Kitabatake, A., 1998. A de novo missense mutation of human cardiac Na+ channel exhibiting novel molecular mechanisms of long QT syndrome. FEBS Letters 423, 5–9.

Makiyama, T., Akao, M., Shizuta, S., Doi, T., Nishiyama, K., Oka, Y., Ohno, S., Nishio, Y., Tsuji, K., Itoh, H., et al., 2008. A novel SCN5A gain-of-function mutation M1875T associated with familial atrial fibrillation. Journal of the American College of Cardiology 52, 1326–1334.

Marangoni, S., Di Resta, C., Rocchetti, M., Barile, L., Rizzetto, R., Summa, A., Severi, S., Sommariva, E., Pappone, C., Ferrari, M., et al., 2011. A Brugada syndrome mutation (p.S216L) and its modulation by p.H558R polymorphism: standard and dynamic characterization. Cardiovascular Research 91, 606–616.

Medeiros-Domingo, A., Kaku, T., Tester, D.J., Iturralde-Torres, P., Itty, A., Ye, B., Valdivia, C., Ueda, K., Canizales-Quinteros, S., Tusié-Luna, M.T., et al., 2007. SCN4B-encoded sodium channel $\beta 4$ subunit in congenital long-QT syndrome. Circulation 116, 134–142.

Medeiros-Domingo, A., Tan, B.H., Iturralde-Torres, P., Tester, D.J., Tusié-Luna, T., Makielski,

J.C., Ackerman, M.J., 2009. Unique mixed phenotype and unexpected functional effect revealed by novel compound heterozygosity mutations involving SCN5A. Heart Rhythm 6, 1170–1175.

Mirams, G.R., Pathmanathan, P., Gray, R.A., Challenor, P., Clayton, R.H., 2016. White paper: Uncertainty and variability in computational and mathematical models of cardiac physiology. The Journal of Physiology (published ahead of print).

Mohler, P.J., Rivolta, I., Napolitano, C., LeMaillet, G., Lambert, S., Priori, S.G., Bennett, V., 2004. NaV1.5 E1053K mutation causing Brugada syndrome blocks binding to ankyrin-G and expression of NaV1.5 on the surface of cardiomyocytes. Proceedings of the National Academy of Sciences of the United States of America 101, 17533–17538.

Mok, N.S., Priori, S.G., Napolitano, C., Chan, N.Y., Chahine, M., Baroudi, G., 2003. A newly characterized SCN5A mutation underlying Brugada syndrome unmasked by hyperthermia. Journal of Cardiovascular Electrophysiology 14, 407–411.

Moreau, A., Krahn, A.D., Gosselin-Badaroudine, P., Klein, G.J., Christé, G., Vincent, Y., Boutjdir, M., Chahine, M., 2013. Sodium overload due to a persistent current that attenuates the arrhythmogenic potential of a novel LQT3 mutation. Frontiers in Pharmacology 4, 126.

Morris, C.E., Juranka, P.F., 2007. NaV channel mechanosensitivity: activation and inactivation accelerate reversibly with stretch. Biophysical Journal 93, 822–833.

Murphy, L.L., Moon-Grady, A.J., Cuneo, B.F., Wakai, R.T., Yu, S., Kunic, J.D., Benson, D.W., George, A.L., 2012. Developmentally regulated SCN5A splice variant potentiates dysfunction of a novel mutation associated with severe fetal arrhythmia. Heart Rhythm 9, 590–597.

Nagatomo, T., Fan, Z., Ye, B., Tonkovich, G., January, C., Kyle, J., Makielski, J., 1998. Temperature dependence of early and late currents in human cardiac wild-type and long QT DeltaKPQ Na+ channels. American Journal of Physiology 275, H2016–H2024.

Nakajima, T., Kaneko, Y., Saito, A., Ota, M., Iijima, T., Kurabayashi, M., 2015. Enhanced fast-inactivated state stability of cardiac sodium channels by a novel voltage sensor SCN5A mutation, R1632C, as a cause of atypical Brugada syndrome. Heart Rhythm 12, 2296–2304.

Nelder, J.A., Mead, R., 1965. A simplex method for function minimization. The Computer Journal 7, 308–313.

Neu, A., Eiselt, M., Paul, M., Sauter, K., Stallmeyer, B., Isbrandt, D., Schulze-Bahr, E., 2010. A homozygous SCN5A mutation in a severe, recessive type of cardiac conduction disease. Human Mutation 31, E1609–E1621.

Nguyen, T.P., Wang, D.W., Rhodes, T.H., George, A.L., 2008. Divergent biophysical defects caused by mutant sodium channels in dilated cardiomyopathy with arrhythmia. Circulation Research 102, 364–371.

O'Leary, M., Digregorio, M., Chahine, M., 2002. Closing and inactivation potentiate the cocaethylene inhibition of cardiac sodium channels by distinct mechanisms. Molecular Pharmacology 64, 1575–1585.

Olesen, M.S., Yuan, L., Liang, B., Holst, A.G., Nielsen, N., Nielsen, J.B., Hedley, P.L., Christiansen, M., Olesen, S.P., Haunsø, S., et al., 2012. High prevalence of long QT syndrome associated SCN5A

variants in patients with early-onset lone atrial fibrillation. Circulation: Cardiovascular Genetics 5, 450.

Otagiri, T., Kijima, K., Osawa, M., Ishii, K., Makita, N., Matoba, R., Umetsu, K., Hayasaka, K., 2008. Cardiac ion channel gene mutations in sudden infant death syndrome. Pediatric Research 64, 482–487.

Passini, E., Mincholé, A., Coppini, R., Cerbai, E., Rodriguez, B., Severi, S., Bueno-Orovio, A., 2016. Mechanisms of pro-arrhythmic abnormalities in ventricular repolarisation and anti-arrhythmic therapies in human hypertrophic cardiomyopathy. Journal of Molecular and Cellular Cardiology 96, 72–81.

Pathmanathan, P., Shotwell, M.S., Gavaghan, D.J., Cordeiro, J.M., Gray, R.A., 2015. Uncertainty quantification of fast sodium current steady-state inactivation for multi-scale models of cardiac electrophysiology. Progress in Biophysics and Molecular Biology 117, 4–18.

Pfahnl, A.E., Viswanathan, P.C., Weiss, R., Shang, L.L., Sanyal, S., Shusterman, V., Kornblit, C., London, B., Dudley, S.C., 2007. A sodium channel pore mutation causing Brugada syndrome. Heart Rhythm 4, 46–53.

Poelzing, S., Forleo, C., Samodell, M., Dudash, L., Sorrentino, S., Anaclerio, M., Troccoli, R., Iacoviello, M., Romito, R., Guida, P., et al., 2006. SCN5A polymorphism restores trafficking of a Brugada syndrome mutation on a separate gene. Circulation 114, 368–376.

Remme, C.A., Wilde, A.A., Bezzina, C.R., 2008. Cardiac sodium channel overlap syndromes: different faces of SCN5A mutations. Trends in Cardiovascular Medicine 18, 78–87.

Rivolta, I., Abriel, H., Tateyama, M., Liu, H., Memmi, M., Vardas, P., Napolitano, C., Priori, S.G., Kass, R.S., 2001. Inherited Brugada and long QT-3 syndrome mutations of a single residue of the cardiac sodium channel confer distinct channel and clinical phenotypes. Journal of Biological Chemistry 276, 30623–30630.

Romero, L., Pueyo, E., Fink, M., Rodríguez, B., 2009. Impact of ionic current variability on human ventricular cellular electrophysiology. American Journal of Physiology – Heart and Circulatory Physiology 297, H1436–H1445.

Rook, M.B., Alshinawi, C.B., Groenewegen, W.A., van Gelder, I.C., van Ginneken, A.C., Jongsma, H.J., Mannens, M.M., Wilde, A.A., 1999. Human SCN5A gene mutations alter cardiac sodium channel kinetics and are associated with the Brugada syndrome. Cardiovascular Research 44, 507–517.

Rossenbacker, T., Carroll, S.J., Liu, H., Kuipéri, C., de Ravel, T.J., Devriendt, K., Carmeliet, P., Kass, R.S., Heidbüchel, H., 2004. Novel pore mutation in SCN5A manifests as a spectrum of phenotypes ranging from atrial flutter, conduction disease, and Brugada syndrome to sudden cardiac death. Heart Rhythm 1, 610–615.

Ruan, Y., Denegri, M., Liu, N., Bachetti, T., Seregni, M., Morotti, S., Severi, S., Napolitano, C., Priori, S.G., 2010. Trafficking defects and gating abnormalities of a novel SCN5A mutation question gene-specific therapy in long QT syndrome type 3. Circulation Research 106, 1374–1383.

Ruan, Y., Liu, N., Bloise, R., Napolitano, C., Priori, S.G., 2007. Gating properties of SCN5A

mutations and the response to mexiletine in long-QT syndrome type 3 patients. Circulation 116, 1137–1144.

Saber, S., Amarouch, M.Y., Fazelifar, A.F., Haghjoo, M., Emkanjoo, Z., Alizadeh, A., Houshmand, M., Gavrilenko, A.V., Abriel, H., Zaklyazminskaya, E.V., 2015. Complex genetic background in a large family with Brugada syndrome. Physiological Reports 3, e12256.

Sakakibara, Y., Furukawa, T., Singer, D.H., Jia, H., Backer, C.L., Arentzen, C.E., Wasserstrom, J.A., 1993. Sodium current in isolated human ventricular myocytes. American Journal of Physiology 265, H1301–H1309.

Sakakibara, Y., Wasserstrom, J.A., Furukawa, T., Jia, H., Arentzen, C.E., Hartz, R.S., Singer, D.H., 1992. Characterization of the sodium current in single human atrial myocytes. Circulation Research 71, 535–546.

Samani, K., Wu, G., Ai, T., Shuraih, M., Mathuria, N.S., Li, Z., Sohma, Y., Purevjav, E., Xi, Y., Towbin, J.A., et al., 2009. A novel SCN5A mutation V1340I in Brugada syndrome augmenting arrhythmias during febrile illness. Heart Rhythm 6, 1318–1326.

Sánchez, C., Bueno-Orovio, A., Wettwer, E., Loose, S., Simon, J., Ravens, U., Pueyo, E., Rodriguez, B., 2014. Inter-subject variability in human atrial action potential in sinus rhythm versus chronic atrial fibrillation. PLOS ONE 9, e105897.

Sarhan, M.F., Van Petegem, F., Ahern, C.A., 2009. A double tyrosine motif in the cardiac sodium channel domain III-IV linker couples calcium-dependent calmodulin binding to inactivation gating. Journal of Biological Chemistry 284, 33265–33274.

Sarkar, A.X., Christini, D.J., Sobie, E.A., 2012. Exploiting mathematical models to illuminate electrophysiological variability between individuals. The Journal of Physiology 590, 2555–2567.

Sarkar, A.X., Sobie, E.A., 2011. Quantification of repolarization reserve to understand interpatient variability in the response to proarrhythmic drugs: a computational analysis. Heart Rhythm 8, 1749–1755.

Schneider, M., Proebstle, T., Hombach, V., Hannekum, A., Rüdel, R., 1994. Characterization of the sodium currents in isolated human cardiocytes. Pflügers Archiv 428, 84–90.

Sherman, A.J., Shrier, A., Cooper, E., 1999. Series resistance compensation for whole-cell patch-clamp studies using a membrane state estimator. Biophysical Journal 77, 2590–2601.

Sherman-Gold, R., Maertz, W.H., 2012. The Axon Guide for Electrophysiology & Biophysics: Laboratory Techniques. Molecular Devices.

Shinlapawittayatorn, K., Du, X.X., Liu, H., Ficker, E., Kaufman, E.S., Deschênes, I., 2011a. A common SCN5A polymorphism modulates the biophysical defects of SCN5A mutations. Heart Rhythm 8, 455–462.

Shinlapawittayatorn, K., Dudash, L.A., Du, X.X., Heller, L., Poelzing, S., Ficker, E., Deschênes, I., 2011b. A novel strategy using cardiac sodium channel polymorphic fragments to rescue trafficking-deficient SCN5A mutations. Circulation: Cardiovascular Genetics 4, 500–509.

Shirai, N., Makita, N., Sasaki, K., Yokoi, H., Sakuma, I., Sakurada, H., Akai, J., Kimura, A.,

Hiraoka, M., Kitabatake, A., 2002. A mutant cardiac sodium channel with multiple biophysical defects associated with overlapping clinical features of Brugada syndrome and cardiac conduction disease. Cardiovascular Research 53, 348–354.

Shuraih, M., Ai, T., Vatta, M., Sohma, Y., Merkle, E.M., Taylor, E., Li, Z., Xi, Y., Razavi, M., Towbin, J.A., et al., 2007. A common SCN5A variant alters the responsiveness of human sodium channels to class I antiarrhythmic agents. Journal of Cardiovascular Electrophysiology 18, 434–440.

Shy, D., Gillet, L., Ogrodnik, J., Albesa, M., Verkerk, A.O., Wolswinkel, R., Rougier, J.S., Barc, J., Essers, M.C., Syam, N., et al., 2014. PDZ domain–binding motif regulates cardiomyocyte compartment-specific NaV1.5 channel expression and function. Circulation 130, 147–160.

Sigworth, F., 1995. Electronic design of the patch clamp, in: Single-channel recording. Springer, pp. 95–127.

Smits, J.P., Koopmann, T.T., Wilders, R., Veldkamp, M.W., Opthof, T., Bhuiyan, Z.A., Mannens, M.M., Balser, J.R., Tan, H.L., Bezzina, C.R., et al., 2005a. A mutation in the human cardiac sodium channel (E161K) contributes to sick sinus syndrome, conduction disease and Brugada syndrome in two families. Journal of Molecular and Cellular Cardiology 38, 969–981.

Smits, J.P., Veldkamp, M.W., Bezzina, C.R., Bhuiyan, Z.A., Wedekind, H., Schulze-Bahr, E., Wilde, A.A., 2005b. Substitution of a conserved alanine in the domain IIIS4–S5 linker of the cardiac sodium channel causes long QT syndrome. Cardiovascular Research 67, 459–466.

Sottas, V., Rougier, J.S., Jousset, F., Kucera, J.P., Shestak, A., Makarov, L.M., Zaklyazminskaya, E.V., Abriel, H., 2013. Characterization of 2 genetic variants of NaV1.5-Arginine 689 found in patients with cardiac arrhythmias. Journal of Cardiovascular Electrophysiology 24, 1037–1046.

Splawski, I., Timothy, K.W., Tateyama, M., Clancy, C.E., Malhotra, A., Beggs, A.H., Cappuccio, F.P., Sagnella, G.A., Kass, R.S., Keating, M.T., 2002. Variant of SCN5A sodium channel implicated in risk of cardiac arrhythmia. Science 297, 1333–1336.

Stewart, P., Aslanidi, O.V., Noble, D., Noble, P.J., Boyett, M.R., Zhang, H., 2009. Mathematical models of the electrical action potential of Purkinje fibre cells. Philosophical Transactions of the Royal Society of London A: Mathematical, Physical and Engineering Sciences 367, 2225–2255.

Surber, R., Hensellek, S., Prochnau, D., Werner, G.S., Benndorf, K., Figulla, H.R., Zimmer, T., 2008. Combination of cardiac conduction disease and long QT syndrome caused by mutation T1620K in the cardiac sodium channel. Cardiovascular Research 77, 740–748.

Swan, H., Amarouch, M.Y., Leinonen, J., Marjamaa, A., Kucera, J.P., Laitinen-Forsblom, P.J., Lahtinen, A.M., Palotie, A., Kontula, K., Toivonen, L., et al., 2014. A gain-of-function mutation of the SCN5A gene causes exercise-induced polymorphic ventricular arrhythmias. Circulation: Cardiovascular Genetics 7, 771–781.

Tan, B.H., Valdivia, C.R., Rok, B.A., Ye, B., Ruwaldt, K.M., Tester, D.J., Ackerman, M.J., Makielski, J.C., 2005. Common human SCN5A polymorphisms have altered electrophysiology when expressed in PQ1077 splice variants. Heart Rhythm 2, 741–747.

Tan, B.H., Valdivia, C.R., Song, C., Makielski, J.C., 2006. Partial expression defect for the SCN5A

missense mutation G1406R depends on splice variant background Q1077 and rescue by mexiletine. American Journal of Physiology – Heart and Circulatory Physiology 291, H1822–H1828.

Tan, H.L., Bink-Boelkens, M.T., Bezzina, C.R., Viswanathan, P.C., Beaufort-Krol, G.C., van Tintelen, P.J., van den Berg, M.P., Wilde, A.A., Balser, J.R., 2001. A sodium-channel mutation causes isolated cardiac conduction disease. Nature 409, 1043–1047.

Tan, H.L., Kupershmidt, S., Zhang, R., Stepanovic, S., Roden, D.M., Wilde, A.A., Anderson, M.E., Balser, J.R., 2002. A calcium sensor in the sodium channel modulates cardiac excitability. Nature 415, 442–447.

Tarradas, A., Selga, E., Beltran-Alvarez, P., Pérez-Serra, A., Riuró, H., Picó, F., Iglesias, A., Campuzano, O., Castro-Urda, V., Fernández-Lozano, I., et al., 2013. A novel missense mutation, I890T, in the pore region of cardiac sodium channel causes Brugada syndrome. PLOS ONE 8, e53220.

Tester, D.J., Valdivia, C., Harris-Kerr, C., Alders, M., Salisbury, B.A., Wilde, A.A., Makielski, J.C., Ackerman, M.J., 2010. Epidemiologic, molecular, and functional evidence suggest A572D-SCN5A should not be considered an independent LQT3-susceptibility mutation. Heart Rhythm 7, 912–919.

Tsurugi, T., Nagatomo, T., Abe, H., Oginosawa, Y., Takemasa, H., Kohno, R., Makita, N., Makielski, J.C., Otsuji, Y., 2009. Differential modulation of late sodium current by protein kinase A in R1623Q mutant of LQT3. Life Sciences 84, 380–387.

ten Tusscher, K.H., Panfilov, A.V., 2006. Alternans and spiral breakup in a human ventricular tissue model. American Journal of Physiology – Heart and Circulatory Physiology 291, H1088–H1100.

Valdivia, C.R., Tester, D.J., Rok, B.A., Munger, T.M., Jahangir, A., Makielski, J.C., Ackerman, M.J., 2004. A trafficking defective, Brugada syndrome-causing SCN5A mutation rescued by drugs. Cardiovascular Research 62, 53–62.

Vatta, M., Dumaine, R., Antzelevitch, C., Brugada, R., Li, H., Bowles, N.E., Nademanee, K., Brugada, J., Brugada, P., Towbin, J.A., 2002a. Novel mutations in domain I of SCN5A cause Brugada syndrome. Molecular Genetics and Metabolism 75, 317–324.

Vatta, M., Dumaine, R., Varghese, G., Richard, T.A., Shimizu, W., Aihara, N., Nademanee, K., Brugada, R., Brugada, J., Veerakul, G., et al., 2002b. Genetic and biophysical basis of sudden unexplained nocturnal death syndrome (SUNDS), a disease allelic to Brugada syndrome. Human Molecular Genetics 11, 337–345.

Viswanathan, P.C., Benson, D.W., Balser, J.R., 2003. A common SCN5A polymorphism modulates the biophysical effects of an SCN5A mutation. The Journal of Clinical Investigation 111, 341–346.

Walch, O.J., Eisenberg, M.C., 2015. Parameter identifiability and identifiable combinations in generalized Hodgkin-Huxley models. arXiv preprint arXiv:1511.05227 .

Wan, X., Chen, S., Sadeghpour, A., Wang, Q., Kirsch, G.E., 2001. Accelerated inactivation in a mutant Na+ channel associated with idiopathic ventricular fibrillation. American Journal of Physiology – Heart and Circulatory Physiology 280, H354–H360.

Wan, X., Wang, Q., Kirsch, G.E., 2000. Functional suppression of sodium channels by β1-subunits

as a molecular mechanism of idiopathic ventricular fibrillation. Journal of Molecular and Cellular Cardiology 32, 1873–1884.

Wang, C., Wang, C., Hoch, E.G., Pitt, G.S., 2011. Identification of novel interaction sites that determine specificity between fibroblast growth factor homologous factors and voltage-gated sodium channels. Journal of Biological Chemistry 286, 24253–24263.

Wang, D.W., Crotti, L., Shimizu, W., Pedrazzini, M., Cantu, F., De Filippo, P., Kishiki, K., Miyazaki, A., Ikeda, T., Schwartz, P.J., et al., 2008. Malignant perinatal variant of long-QT syndrome caused by a profoundly dysfunctional cardiac sodium channel. Circulation: Arrhythmia and Electrophysiology 1, 370–378.

Wang, D.W., Desai, R.R., Crotti, L., Arnestad, M., Insolia, R., Pedrazzini, M., Ferrandi, C., Vege, A., Rognum, T., Schwartz, P.J., et al., 2007a. Cardiac sodium channel dysfunction in sudden infant death syndrome. Circulation 115, 368–376.

Wang, D.W., Viswanathan, P.C., Balser, J.R., George, A.L., Benson, D.W., 2002. Clinical, genetic, and biophysical characterization of SCN5A mutations associated with atrioventricular conduction block. Circulation 105, 341–346.

Wang, D.W., Yazawa, K., George, A.L., Bennett, P.B., 1996. Characterization of human cardiac Na+ channel mutations in the congenital long QT syndrome. Proceedings of the National Academy of Sciences 93, 13200–13205.

Wang, H.G., Zhu, W., Kanter, R.J., Silva, J.R., Honeywell, C., Gow, R.M., Pitt, G.S., 2016. A novel NaV1.5 voltage sensor mutation associated with severe atrial and ventricular arrhythmias. Journal of Molecular and Cellular Cardiology 92, 52–62.

Wang, L., Meng, X., Yuchi, Z., Zhao, Z., Xu, D., Fedida, D., Wang, Z., Huang, C., 2015. De novo mutation in the SCN5A gene associated with Brugada syndrome. Cellular Physiology and Biochemistry 36, 2250–2262.

Wang, S.Y., Tikhonov, D.B., Mitchell, J., Zhorov, B., Wang, G.K., 2007b. Irreversible block of cardiac mutant Na+ channels by batrachotoxin. Channels 1, 179–188.

Watanabe, H., Yang, T., Stroud, D.M., Lowe, J.S., Harris, L., Atack, T.C., Wang, D.W., Hipkens, S.B., Leake, B., Hall, L., et al., 2011a. Striking in vivo phenotype of a disease-associated human SCN5A mutation producing minimal changes in vitro. Circulation 124, 1001–1011.

Watanabe, H., Yang, T., Stroud, D.M., Lowe, J.S., Harris, L., Atack, T.C., Wang, D.W., Hipkens, S.B., Leake, B., Hall, L., et al., 2011b. Striking in vivo phenotype of a disease-associated human SCN5A mutation producing minimal changes in vitro. Circulation 124, 1001–1011.

Wedekind, H., Smits, J.P., Schulze-Bahr, E., Arnold, R., Veldkamp, M.W., Bajanowski, T., Borggrefe, M., Brinkmann, B., Warnecke, I., Funke, H., et al., 2001. De novo mutation in the SCN5A gene associated with early onset of sudden infant death. Circulation 104, 1158–1164.

Wehrens, X.H., Rossenbacker, T., Jongbloed, R.J., Gewillig, M., Heidbüchel, H., Doevendans, P.A., Vos, M.A., Wellens, H.J., Kass, R.S., 2003. A novel mutation L619F in the cardiac Na+ channel SCN5A associated with long-QT syndrome (LQT3): a role for the I-II linker in inactivation gating. Human Mutation 21, 552–552.

Wei, J., Wang, D.W., Alings, M., Fish, F., Wathen, M., Roden, D.M., George, A.L., 1999. Congenital long-QT syndrome caused by a novel mutation in a conserved acidic domain of the cardiac Na+ channel. Circulation 99, 3165–3171.

Weiss, J.N., Garfinkel, A., Karagueuzian, H.S., Nguyen, T.P., Olcese, R., Chen, P.S., Qu, Z., 2015. Perspective: A dynamics-based classification of ventricular arrhythmias. Journal of Molecular and Cellular Cardiology 82, 136–152.

Weiss, J.N., Karma, A., MacLellan, W.R., Deng, M., Rau, C.D., Rees, C.M., Wang, J., Wisniewski, N., Eskin, E., Horvath, S., Qu, Z., Wang, Y., Lusis, A.J., 2012. "Good enough solutions" and the genetics of complex diseases. Circulation Research 111, 493–504.

Willms, A.R., Baro, D.J., Harris-Warrick, R.M., Guckenheimer, J., 1999. An improved parameter estimation method for Hodgkin-Huxley models. Journal of Computational Neuroscience 6, 145–168.

Winkel, B.G., Larsen, M.K., Berge, K.E., Leren, T.P., Nissen, P.H., Olesen, M.S., Hollegaard, M.V., Jespersen, T., Yuan, L., Nielsen, N., et al., 2012. The prevalence of mutations in KCNQ1, KCNH2, and SCN5A in an unselected national cohort of young sudden unexplained death cases. Journal of Cardiovascular Electrophysiology 23, 1092–1098.

Yang, P., Kanki, H., Drolet, B., Yang, T., Wei, J., Viswanathan, P.C., Hohnloser, S.H., Shimizu, W., Schwartz, P.J., Stanton, M., et al., 2002. Allelic variants in long-QT disease genes in patients with drug-associated torsades de pointes. Circulation 105, 1943–1948.

Ye, B., Valdivia, C.R., Ackerman, M.J., Makielski, J.C., 2003. A common human SCN5A polymorphism modifies expression of an arrhythmia causing mutation. Physiological Genomics 12, 187–193.

Yokoi, H., Makita, N., Sasaki, K., Takagi, Y., Okumura, Y., Nishino, T., Makiyama, T., Kitabatake, A., Horie, M., Watanabe, I., et al., 2005. Double SCN5A mutation underlying asymptomatic Brugada syndrome. Heart Rhythm 2, 285–292.

Young, K.A., Caldwell, J.H., 2005. Modulation of skeletal and cardiac voltage-gated sodium channels by calmodulin. The Journal of Physiology 565, 349–370.

Zeng, Z., Zhou, J., Hou, Y., Liang, X., Zhang, Z., Xu, X., Xie, Q., Li, W., Huang, Z., 2013. Electrophysiological characteristics of a SCN5A voltage sensors mutation R1629Q associated with Brugada syndrome. PLOS ONE 8, e78382.

Zhang, J., Chen, Y., Yang, J., Xu, B., Wen, Y., Xiang, G., Wei, G., Zhu, C., Xing, Y., Li, Y., 2015. Electrophysiological and trafficking defects of the SCN5A T353I mutation in Brugada syndrome are rescued by alpha-allocryptopine. European Journal of Pharmacology 746, 333–343.

Zhang, Y., Wang, T., Ma, A., Zhou, X., Gui, J., Wan, H., Shi, R., Huang, C., Grace, A., Huang, C.H., et al., 2008. Correlations between clinical and physiological consequences of the novel mutation R878C in a highly conserved pore residue in the cardiac Na+ channel. Acta Physiologica 194, 311–323.